LEVEL II

(11)

AD A095341

SECURITY CLASSIFICATION OF THIS PAGE (When Data Entered)

REPORT DOCUMENTATION PAGE	READ INSTRUCTIONS BEFORE COMPLETING FORM
1. REPORT NUMBER: 5 ✓	2. GOVT ACCESSION NO.: AD-A095 341
3. RECIPIENT'S CATALOG NUMBER	
4. TITLE (and Subtitle): Theoretical Study of Atom Surface Interactions	5. TYPE OF REPORT & PERIOD COVERED: Technical Report - Final 1975-1980
	6. PERFORMING ORG. REPORT NUMBER
7. AUTHOR(s): Narkis Tzoar	8. CONTRACT OR GRANT NUMBER(s): N00014-75-C-0949 ✓
9. PERFORMING ORGANIZATION NAME AND ADDRESS: The City College, New York, N.Y.	10. PROGRAM ELEMENT, PROJECT, TASK AREA & WORK UNIT NUMBERS: NR 392-012
11. CONTROLLING OFFICE NAME AND ADDRESS: Office of Naval Research, Arlington, Va. 22217	12. REPORT DATE: Feb. 1981
	13. NUMBER OF PAGES
14. MONITORING AGENCY NAME & ADDRESS (if different from Controlling Office): Office of Naval Research (Code 434), 800 North Quincy St., Arlington, Va. 22217	15. SECURITY CLASS. (of this report): Unclassified
	15a. DECLASSIFICATION/DOWNGRADING SCHEDULE

16. DISTRIBUTION STATEMENT (of this Report)

Approved for public release; distribution unlimited.

DTIC
FEB 23 1981
C

17. DISTRIBUTION STATEMENT (of the abstract entered in Block 20, if different from Report)

18. SUPPLEMENTARY NOTES

Summary of Research on Electron Stimulated Desorption

19. KEY WORDS (Continue on reverse side if necessary and identify by block number)

Theoretical Study
Surfaces
Electron Stimulated Desorption
Photodesorption
Kinetic Theory
Conductivity

DOCUMENT IS BEST QUALITY PRACTICABLE.
THE COPY FURNISHED TO DDC CONTAINED A
SIGNIFICANT NUMBER OF PAGES WHICH DO NOT
REPRODUCE LEGIBLY.

20. ABSTRACT (Continue on reverse side if necessary and identify by block number)

A first principles kinetic theory was developed, applicable to angular and energy dependent emission in Electron Stimulated Desorption. Expressions for the ionic and neutral atoms ESD cross section were formulated and applied in a model calculations of O^+ emission from W(100) and W(111). Strong focussing of the outgoing ions was found. Off-axis spot groups were simulated and compared with experimental results.

81 2 20 02

DD FORM 1 JAN 73 1473 EDITION OF 1 NOV 65 IS OBSOLETE
S/N 0102-LF-014-6601

SECURITY CLASSIFICATION OF THIS PAGE (When Data Entered)

DDC FILE COPY

(14) TR-5

(9) FINAL SCIENTIFIC REPORT.

1 Jul 75 — 31 Dec 80

(6) THEORETICAL STUDIES OF ATOM SURFACE INTERACTIONS.

(10) Narkis/Tzoar
Dept. of Physics
The City College of The City University
of New York
New York, N.Y. 10031

(11) Feb 81 (12) 67

(15) N00014-75-C-0949

404398

FINAL SCIENTIFIC REPORT

TITLE: THEORETICAL STUDIES OF ATOM-SURFACE INTERACTIONS

Grant No. ONR N00014-75-C-0949

Principal Investigator: Professor Narkis Tzoar

The City College of The City University of New York

The main thrust of our research was to investigate the desorption of atoms from solid state surfaces. Interest in atom desorption stems from several sources. First it provides a tool for characterizing surfaces. One may identify and measure the amounts of various adsorbates on a surface and learn the elementary physical and chemical processes associated with their bonding. Secondly, as a technological tool, desorption provides technique for preparing and cleaning a surface. Thirdly, the degradation of the surface and underlying substrate of the walls by radiation or particle bombardment become a matter of practical concern in many situations. Also desorption of atoms from the surfaces of interstellar dust grains provides a mechanism for the coupling of radiant energy from stars to the kinetic energy interstellar atoms or molecules. Desorption is thus a phenomenon of rather universal concern and of practical interest in many branches of physics and chemistry.

Experimental and theoretical developments related to this project were reviewed recently, in the November 1980 issue of Physics Today (see Search and Discovery column).

One may regard desorption as a collision process in which an incident projectile collides with an adatom and ejects it. If the incident particle is an ion the process is known as sputtering. If

the incident particle is an electron or photon, it termed electron stimulated desorption or photodesorption respectively. Thermaldesorption may be thought of as a collision process involving incident thermally excited phonons.

The main efforts during the first half of the grant duraction was two fold: (a) to develop the kinetic theory of the ion distribution in electron stimulated desorption (ESD), (b) to determine the potential energy curves which repel the ions away from the host surface.

Our kinetic theory assumes, for simplicity, a two level system i.e. an energy curve for the adatom which determines its ground state and an excited (repulsive) energy state for the adatom's ion. The parameters which determine these energy curves will be considered shortly. We then obtain the coupled Boltzmann equations for the deviation of the probability from equilibrium for finding the adatom in one of the two states as:

$$\frac{\partial P_2}{\partial t} + \vec{v}\cdot\nabla P_2 - \frac{1}{M}\nabla E_2 \cdot \frac{\partial P_2}{\partial \vec{v}} = (\dot{P}_2)_E - (\dot{P}_2)_Q$$
$$\frac{\partial P_1}{\partial t} + \vec{v}\cdot\nabla P_1 - \frac{1}{M}\nabla E_1 \cdot \frac{\partial P_1}{\partial \vec{v}} = (\dot{P}_2)_Q \qquad (1)$$

Here E_1 (E_2) is the energy curve of the ground (excited) state and the subscripts "E" and "Q" stands for "Excitation" (by the incoming electron) and "Quenching". The source term $(P_2)_E$ is taken to be weak thus:

$$(\dot{P}_2)_E = P_0 R \qquad (2)$$

Where R is a rate given from scattering theory and P_o represents the ground state of the adatom. The quenching term is taken to be

Accession For
NTIS GRA&I
DTIC TAB
Unannounced
Justification
By
Distribution/
Availability Codes
Dist | Avail and/or Special

$$(\dot{P}_2)_Q \simeq P_2\, Q(r) \tag{3}$$

where, for example, one may take

$$Q(r) = \frac{1}{T_Q}\, e^{-z/\lambda}$$

Here T_Q is an average quenching time on the substrate surface and λ represent the range of the "substrate" electrons away from the surface. We thus may write the kinetic equation as:

$$\frac{\partial P_2}{\partial t} + \bar{v}\cdot\nabla P_2 - \frac{1}{M}\nabla E_2 \cdot \frac{\partial P_2}{\partial \bar{v}} = P_0 R - P_2 Q$$

$$\frac{\partial P_1}{\partial t} + \bar{v}\cdot\nabla P_1 - \frac{1}{M}\nabla E_1 \cdot \frac{\partial P_1}{\partial \bar{v}} = P_2 Q \tag{4}$$

This set of equations yields the angular and energy dependence, linear in the incident flux, in terms of the energy curves (E_1, E_2), the excitation rate (R) and the quenching (Q).
In view of the complexities associated with the solution of Eq. (4), we adopt an approach well suited to numerical simulation of ESD ion angular and energy distributions.

The steady state ESD response is found by solving an equivalent time dependent problem. We simulate the flux of ions or neutral atoms desorbed in response to an incident electron pulse of short duration τ, then take the limit $\tau \longrightarrow 0$. We obtain below suitable expressions for the total desorption cross sections, using the transport formulation. Numerical differentiation in the asymptotic

plane allows one to recover the angular dependence.

We employ the time ordered picture of ESD in implementing this strategy. An ensemble of absorbed ground state atoms is perturbed at t = 0 by the electron beam. The forward evolution of the system is followed, without further interaction with the external beam, to a time t large enough for all ions or reneutralized atoms which can desorb to have crossed a detection plane. Each trajectory must be individually followed to its asymptotic direction via the classical equations of motion. One evaluates each ion's or atom's contribution to the cross section, including attenuation due to quenching.

Time dependent solutions of the kinetic equations are required. Hence, we obtain formal solutions for P_n which map the evolution of an initial distribution function forward in time. These are then used to construct the desorption cross sections.

By convention, we suppress the dependence of all quantities on r, v, displaying only their parametric time dependence. The classical dynamics problem will be solved numerically. Liouville's Theorem prompts us to replace

$$\frac{\partial}{\partial t} + \bar{v} \cdot \nabla + \bar{a} \cdot \frac{\partial}{\partial \bar{v}} \rightarrow \frac{d}{dt}$$

after which they take the form:

$$\frac{dP_2'}{dt} = P_1^0(t) R(t) - Q(t) P_2'(t)$$

$$\frac{dP_1'}{dt} = P_2'(t) Q(t)$$

First, we introduce the ionic survival probability against reneutralization, $S_2(t_o,t)$, which is defined to be:

$$S_2(t_o,t) = \exp\left\{-\int_{t_o}^{t} dt' Q(t')\right\}$$

The exponent is the reneutralization rate integrated along the ionic trajectory from $r(t_o)$ to $r(t)$, which is governed by $E_2(r)$. An alternative notation which displays the path integration explicitly is:

$$S_2(\vec{r}_o,\vec{r}) = \exp\left\{-\int_{\vec{r}_o}^{\vec{r}} \vec{v}(\vec{r}')\cdot d\vec{r}'\, Q(r')/|v(\vec{r}')|^2\right.$$

Here, $v(r')$ is the ionic velocity at r'. It is useful to interpret $S_2(t_o,t)$ as an evolution operator, which maps ions from their initial to final coordinates.

ESD cross sections are experimentally found to be several orders of magnitude smaller than atomic ionization cross sections would indicate (1,2). Hence, quenching is presumed to be important and we expect $S_2(t_o,t) \ll 1$, when $\vec{r}(t_o)$ is close to the surface, and $r(t)$ lies in the detection plane. It is also clear that $S_2(t_o,t) = S_2(t,t') = S_2(t_o,t) = S_2^{-1}(t,t_o)$.

We adopt the following trial solution for $P_2^1(t)$.

$$P_2^1(t) \equiv g(t) S_2(t_o,t)$$

After formally differentiating the above we find that the unknown function $g(t)$ satisfies:

$$\frac{dg(t')}{dt'} = R(t') P_1^o(t') S_2^{-1}(t_o,t)$$

The formal solution $P_2^1(t)$ for the ionic state is found to be:

$$P_2'(t) = P_2'(t_0) S_2(t_0,t) + P_1^\circ(t_0) \int_{t_0}^{t} dt' R(t') S_2(t',t)$$

Here, we integrated the equation for g(t) formally over $t_0 \leq t' \leq t$. The boundary condition $g(t_0) = P_2^1(t_0)$ is found by taking the limit $t \to t_0 + \epsilon$. One notes that $\lim_{t \to t_0} S_2(t_0,t) = 1$. Both R(t), Q(t) are assumed to be mathematically well behaved. The equilibrium distribution satisfies $P_1^\circ(t) = P_1^\circ(t_0)$.

Our solution for $P_2^1(t)$ yields the ionic distribution function which has evolved from the initial distributions $P_2^1(t_0)$ and $P_1^\circ(t_0)$. The first term displays attenuation of the initial ion density, while the second incorporates ionizations which occur during the interval $[t_0,t]$.

The formal solution containing the ground state component of quenched particles, is:

$$P_1'(t) = P_1'(t_0) + \int_{t_0}^{t} dt' \; P_2'(t') Q(t')$$

Here, one uses the state 1 dynamics to map $\vec{r}(t')$, $\vec{v}(t')$ forward to time t in the second term.

We commence construction of the cross sections by first examining the response of a single ground state adatom to ionizing transitions during the short finite interval $[-\tau, o]$. Let $U^+(-P,o)$ be the probability of finding the atom as an ion at t = 0. This is found to be:

$$U^+(-\tau, o) = \int_{-\tau}^{0} dt' \; R(t') \; S_2(t',0)$$

Here we chose $P_2^1(-\tau) = 0$, inasmuch as the initial ionic population must be excluded from the response during $[-\tau, o]$. We normalized to unit source strength with the choice $P_1^o(t_o) = 1$. The explicit of U^+ is fixed by the choice of initial conditions $\vec{r}(-\tau)$, $\vec{v}(-\tau)$.

Next, we examine the evolution of a single ion from t = 0 to time t, when its velocity has reached the asymptotic value. No further interaction with the external electrons is permitted to occur; hence, we choose $P_1^o(t_o = o) = o$, $P_2^1(t_o = 0) = 1$. Conditional probabilities for finding the atom with $\vec{r}(t)$, $\vec{v}(t)$ are given by:

$$V^+(0,t) = S_2(0,t)$$

for the ionic state, and

$$V^o(0,t) = \int_0^t dt' S_2(0,t') Q(t')$$

for the ground state. An ion may reneutralize at any time after t = o. Hence, $V^o(o,t)$ contains an integration over intermediate times.

Next, we identify single atom ejection probabilities $T^{+,o}(-\tau,0,t)$ in the ionic and neutral state. These follow the history of an adsorbed atom which responds to the external beam over $[-\tau,o]$:

$$T^+(-\tau,0,t) = U^+(-\tau,0)V^+(0,t)$$

$$T^o(-\tau,0,t) = U^+(-\tau,0)V^o(0,t)$$

These quantities are closely related to the ionic and neutral atom desorption cross sections to be presented below.

New we introduce the ionization cross section $\chi(\vec{r}_o)$ for an adsorbed atom at the point $\vec{r} = \vec{r}(t=0)$. This function must have the free atomic or molecular ionization cross section as its limit when $z_o \to \infty$. Here, ϵ is the incident electron energy. We expect $\chi(\vec{r}_o)$ to be linear in the upward transition rate R_ϵ as follows:

$$\chi_\epsilon(\vec{r}_o) = R_\epsilon(\vec{r}_o)/F$$

This result is recovered after first noting that $U^+(-\tau,o)/\tau$ is the average ionization rate per atom. The corresponding average ionization cross section per atom is given by:

$$\bar{\chi}_\epsilon(-\tau,0) = \frac{1}{F\tau}\int_{-\tau}^{0} dt' R_\epsilon(t') S_2(t',0)$$

Now the limit $\tau \to o^+$ is taken, to obtain the instantaneous response. $R(t')$ is smoothly varying for ESD, inasmuch as the summations over final state electron coordinates contained in R_ϵ consume any delta function resonances. One factors $R_\epsilon(t' = 0)$ from the integration above, and makes the replacement $S_2(t',0) \approx S_2(-\tau,0) = 1$.

The cross section for the entire process resulting in ionic desorption of an atom initially in the ground state is given by:

$$\sigma_{EJ}^{+}(0,t) = \chi_\epsilon(\vec{r}_o) V^+(0,t)$$
$$= \frac{1}{F} R_\epsilon(\vec{r}_o) \exp\left(-\int_0^t dt' Q(t')\right) \theta\left[\frac{mv_o^2}{2} + E_2(\vec{r}_o) - E_2(\infty)\right]$$

Here, we explicitly display the dependence on R and Q. The step function was inserted to ensure that desorption is energetically possible. One integrates the decay probability appearing in the

exponent from point to point as the trajectory is followed. The asymptotic velocity generated by σ_{EJ}^{+} depends on the choice of $\vec{r}(0)$, $\vec{v}(o)$. One chooses t for each ion path so that z(t) lies far from the surface.

The analogous ground state ejection cross section is given by:

$$\sigma_{EJ}^{o}(0,t) = \chi_\epsilon(\vec{R}_0)\, V^o(0,t)$$
$$= \chi_\epsilon(\vec{R}_0) \int_0^t dt' \exp\left\{-\int_0^{t'} dt'' Q(t'')\right\} Q(t') \cdot$$
$$\cdot \Theta\left[\frac{mv_0^2}{2} + E_2(\vec{R}_0) - E_2(\vec{R}') + E_1(\vec{R}') - E_1(\infty)\right]$$

Here, we inserted a step function at the reneutralization point to eliminate trapped particles. E_2 governs the path integrations during $(0,t')$, while E_1 determines the dynamics during (t',t). Numerical evaluation of σ_{EJ}^{o} is expected to be time consuming due to the integration on intermediate times.

Finally, we ensemble average the ejection cross sections over the phase space coordinates at t = 0. The formal solutions which yield the total ionic and neutral atom ESD cross sections are:

$$\sigma^{+}(\epsilon) = \int d\vec{R}_0\, d\vec{v}_0\, P_1^o(\vec{R}_0,\vec{v}_0)\, \chi_\epsilon(\vec{R}_0)\, S_2(0,t)\, \Theta\left[\frac{mv_\parallel^2}{2} + E_2(\vec{R}_0) - E_2(\infty)\right]$$

$$\sigma^{o}(\epsilon) = \int d\vec{R}_0\, d\vec{v}_0\, P_1^o(\vec{R}_0,\vec{v}_0)\, \chi_\epsilon(\vec{R}_0) \int_0^t dt'\, S_2(0,t')\, Q(t') \cdot$$
$$\cdot \Theta\left[\frac{mv_0^2}{2} + E_2(\vec{R}_0) - E_2(\vec{R}') + E_1(\vec{R}') - E_1(\infty)\right]$$

The equilibrium distribution P_1^o was used in averaging, rather than P_1, inasmuch as the ejection cross sections are already linear in R. We apply our expression for σ^{+} below, to numerical simulation of ESDIAD for O^{+} adsorbed on Tungsten.

Note that the equation for σ^{+} is a generalization of phenomenological expressions which have appeared in the literature..

Our previous work on one dimensional photodesorption theory produced analogous forms for the optically fluorescent and ground state cross sections.

The result expressed above is model independent, except for general restrictions on R, Q, E_n, and P_1^o outlined previously. One may use the above equation in conjunction with realistic model surface interactions to obtain ESDIAD patterns and energy spectra within the Menzel-Gomer, Redhead ESD picture.

Finally, we note that the transport approach is applicable to a wide variety of surface phenomena involving propagation of atoms, ions or molecules. In particular, the cross section contributions to higher order excitation processes in ESD may be obtained without difficulty.

Model for Ionic ESD of Oxygen from Tungsten

We solve the kinetic equations using the following assumptions, for simplicity. These do not change the qualitative nature of our solution. We neglect, for the time being all quenching effects, and take R to be constant. The energy curve E_1 is chosen to be

$$E_1(\vec{r}) = -V_0 + \frac{1}{2}\,(\vec{r}-\vec{b})\cdot\overleftrightarrow{K}\cdot(\vec{r}-\vec{b})$$

where $K_{\alpha\beta}$ are fitted to best experimental "spring constants". The excited state energy curve $E_2(r)$ has an attractive (toward the substrate) image potential and a Hartree potential due to the tungsten atoms located on the lattice sites. Thus (in atomic units)

$$V_I = \sum_{\ell} V_a\,(\vec{r}-\vec{R}_\ell) - \frac{1}{4z + d(R_s)}$$

and

$$V_a(\vec{r}) = 7.7\, e^{-1.3r}$$

An alternative (and opposite) approach to the ion potential is given by treating the tungsten atoms, or lattice positions as a core ions with Z = 6 and letting the 6 (2S, 4d) electrons provide the screening using Thermes-Fermi linearized theory. The strength and range of the ionic potential are about the same as obtained using for the localized tungsten atomic wave functions.

The conclusion of our calculations indicates a large focusing effect of ions due to the substrate potential.

The first phase of our calculation was carried out for the desorption from O_2/W. In our Phys. Rev. Lett. 36, 610 (1976), we present the angular distribution curves of O^+, from W(100) surfaces. We thereafter improve our computational capability, verified our W(100). results and obtained new results for the angular distribution curves of O^+ from W(111) which we have presented in Surface Science 69, 253 (1977). The most attractive feature of our calculations has been to show from first principles the large focusing effect on the ions which results in sharp angular patterns that can be traced to the ion-solid potential. We have also been able to show that for geometries where strong focusing occurs the dominant part of the repulsive potential is due to the nearest metal atom or atoms. One difficulty, however, has been in the choice of the interaction potential. Due to the lack of realistic potential curves we have adopted the simplest possible potential imaginable - that

is a linear combination of the ground state atomic Hartree potential augumented by an image potential. There are indications that this potential may not differ much from the potential surrounding a realistic solid and thus it would reasonably represent the ion-solid interaction. It was concluded that while theory predicts for O^+ from O_2/W that ions should emerge predominantly with energies of 2-4 eV, experiments have indicated that most ions are ejected typically with energies of the order of 8 eV. We have made an extensive survey of the experimental literature and have found that the maximum kinetic energy of desorbed O^+ from O_2/N_i O_2/Si and O_2/Ge is about the same as for O_2/W which is approximately 12 eV. (See our paper Phys. Rev. 16B, 945 (1977)). Repulsive energy of 12 eV can be accounted for by the existence of O_2^{++}. Although our speculation that the observed O^+ results from a small number of non-dissociative O_2 may not be correct, our main observation that the large kinetic energy of the O^+ ions may result from doubly (or triply) ionized "molecular complex" on the surface is yet an open question, and as we believe may yet turn out to be true. The model of Auger induced desorption for ionic crystals proposed by Knotek and Fiebelman (Phys. Rev. Lett. 40, 964 (1978)) may prove to be correct also for covalent as well as ionic bonding. It is clear that the two-or three-hole intermediate state which results from the Auger process of core ionization for covalent bonding will be long-lived only if many body effects are dominant. To date the later is also an open question.

Prompted in large measure by our finding for O^+ desorbed from O_2/W, we have studied the ESD of H^+ from H_2/W. Here the

metallic characteristics of the tungsten substrate are preserved and electronic excitations are likely to disappear in times shorter than the desorbing time. Our results (Surface Science, 75, L766 (1978)) for the energy curves of H^+ from H_2/W support the picture of ESD proposed by Gomer, Menzel and Readhead.

Our research has widened to optic and electronic properties of surfaces. We have calculated the interaction of polar-optical phonons with a two dimensional electron gas (Surface Science, 84, 440 (1979)) and have used this result to obtain the high frequency conductivity of a two-dimensional electron gas interacting with optical phonons (Phys. Rev. 20B, 1306 (1979)). This result is useful for "Metal-Oxide-Semiconductors" devices for polar semiconductors. We heave also investigated from first principles the high-frequency conductivity of a two-dimensional, two-component electron gas (Phys. Rev. 20B, 4189 (1979)). Here we have considered the effects of electron-electron correlations on the conductivity. Our result is applicable again for "Metal-Oxide-Semiconductor" devices for multi-valley semiconductors.

At present we are investigating the following work: (a) the high temperature effects on surface absorption in metallic reflectors for high power laser use, (b) the effect of energy loss of charged particles due to coupling to surface vibrations at low incident energies, and (c) pumping of resonant vibration mode of admolecules on a substrate for very short pulses.

0457C

THEORY OF ION ANGULAR DISTRIBUTIONS IN ELECTRON-STIMULATED DESORPTION

Joel I. Gersten, Richard Janow, and Narkis Tzoar

Reprinted from PHYSICAL REVIEW LETTERS Vol. 36, No. 11, 15 March 1976
610

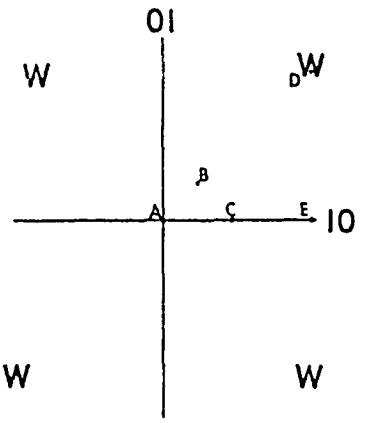

FIG. 1. Sketch of the (100) face of tungsten with several reference points labeled. W denotes the tungsten atoms.

domly selected according to a Maxwell-Boltzmann distribution. The atoms are converted to ions (by the excitation process) and follow an appropriate dynamic trajectory. The asymptotic direction of the ion is recorded and displayed in the figures to follow. For those cases where sharp cones occur, the effect of surviving the quenching process just leads to a constant-numerical-factor correction. Since we will not discuss absolute cross sections here but only the angular distributions, we will neglect such numerical factors. For those distributions which are broader in extent the effect of quenching will be to reduce sharply the flux of wide angle ions. This effect has been discussed in the literature[3] and has to do with the amount of time spent in the vicinity of the surface.

In Fig. 1 we present a sketch of the (100) surface of tungsten. Various points on the surface have been labeled for reference purposes. Let us start by examining the angular patterns produced by assuming a single adatom lies on the substrate. In Fig. 2(a) we present the spot pattern produced by assuming that the original atom was centered at point A at a distance of 1 Bohr from the surface. Figure 2(b) shows the spot pattern when the atom is located at position D a distance of 4 Bohr from the surface (both positions corresponding to realistic[8] W-O bond lengths). We see that the spot patterns do not have lobes. Positions A and D are high-symmetry points where the potential surfaces have approximate cylindrical symmetry. Thus there is no reason for preferred azimuthal emission directions to occur. A similar result has been found for the atom at point E, a distance of 3.0 Bohr above the surface. In the low-coverage phase (β_2 phase) it has been conjectured that the atoms go into position D and no sharp lobes have been found experimentally, although there appears to be a hint of a hazy cross pattern.[3]

In Fig. 3(a) we present the spot pattern associated with the atom lying originally at point B (coordinates $x=0.7a_0$, $y=0.7a_0$, $z=1.0a_0$, where $a=5.97a_0$ is the tungsten lattice constant). Here we see sharp islands appear. The angular patterns have a fourfold rotational symmetry and a fourfold reflection symmetry—resulting in a replication of the pattern of the first octant in the other seven octants. In Fig. 3(b) the spot pattern associated with point C ($x=1.4a_0$, $y=0$, $z=1.0a_0$) is presented. The pattern also displays sharp cones but rotated by an angle of $\pi/4$. In both

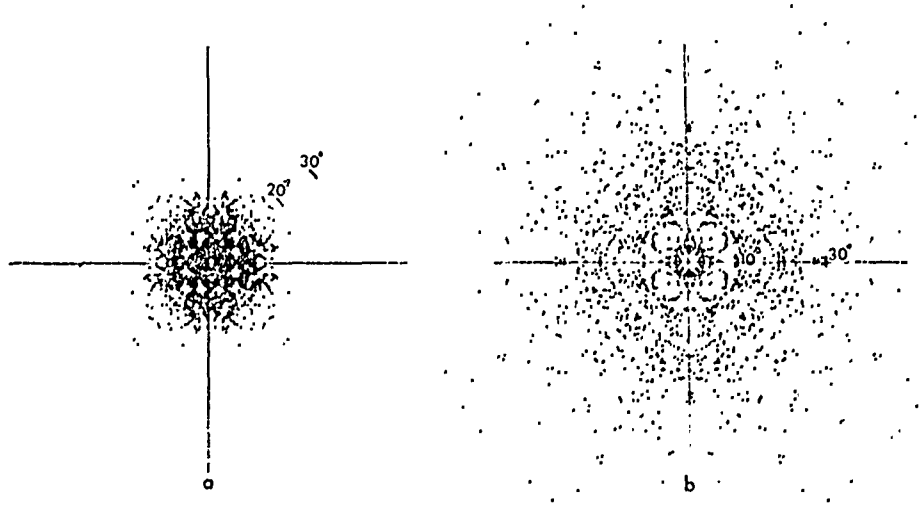

FIG. 2. Spot patterns corresponding to reference points A and D of Fig. 1.

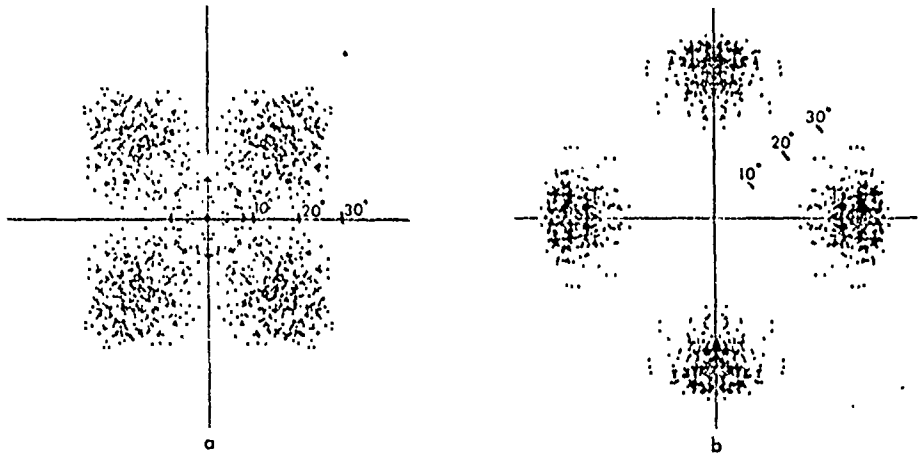

FIG. 3. Spot patterns corresponding to reference points B and C of Fig. 1.

cases the upper-state potential surface is highly anisotropic and thus the dynamical evolution of the trajectories could be expected to produce sharp angular patterns. The degree of angular divergence of the cones as well as their size depend on both the distance away from the surface and the distance away from symmetry points in the plane of the surface. Since we are using a rather crude ionic potential we shall not explore the systematics of the variation here. However if a more accurate ion-solid potential were available, one should be able to pin down the approximate location of the adatom.

One must emphasize that the spot patterns are not unique to the geometries cited above. If one now looks at situations where there are two adatoms (e.g., an O_2 molecule) adsorbed on the surface, it is possible that the second oxygen atom provides an asymmetric potential for the ion to be accelerated by. In Fig. 4(a) we show the spot pattern resulting from a molecule situated at point D with orientation parallel to the [10] direction. In Fig. 4(b) we have the molecule rotated by an angle of $\pi/4$ in the surface plane. The interatomic oxygen distance has been taken to be that appropriate to molecular oxygen. Since experimentally the cones are associated with the β_1 phase of adsorbed oxygen and since this phase is believed to involve molecular oxygen, we see that a reasonable explanation can be had in the context of such a model.

In summary we have shown that the angular patterns can be explained in terms of the dynamics of the ion-solid interaction. Two possibilities exist to explain the patterns. Both involve the three-dimensional spatial asymmetry of the potential seen by the oxygen ion when it is produced. The first situation involves a single atom located

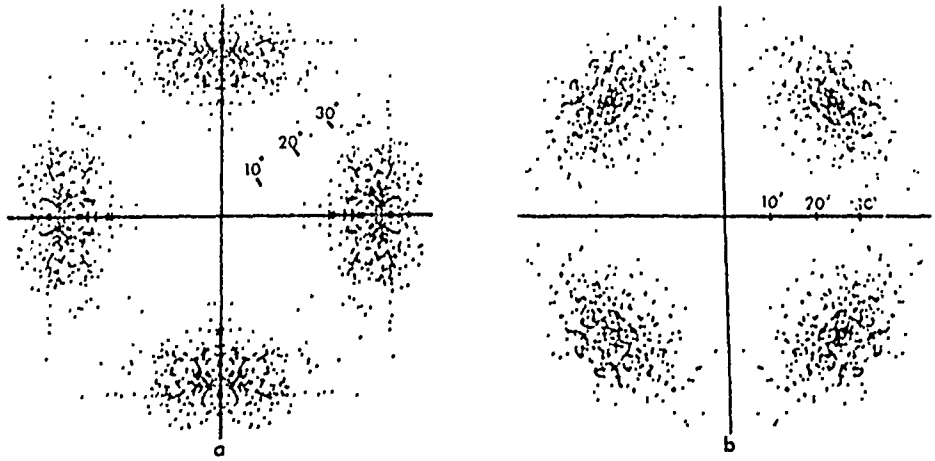

FIG. 4. Spot patterns corresponding to desorption from molecular oxygen.

at a nonsymmetry site. Such a nonconventional location could be brought about by subtle long-range interactions between oxygen atoms on the surface. The second situation involves an oxygen molecule pinned to a tungsten atom on the surface. The present theory is not able to differentiate between these cases. Thus further diagnostics and analysis are necessary. Currently we are investigating the possibility that vacancies in an oxygen overlayer could give rise to additional potential asymmetries.

*Research sponsored by the U. S. Office of Naval Research under ONR Contract No. N00014-75-C-0949.

[1]For recent reviews see D. Menzel, Surf. Sci. 47, 370 (1975); T. E. Madey and J. T. Yates, Jr., J. Vac. Sci. Technol. 8, 525 (1971).

[2]P. A. Redhead, Can. J. Phys. 42, 886 (1964); D. Menzel and R. Gomer, J. Chem. Phys. 41, 3311 (1964).

[3]T. E. Madey, J. J. Czyzewski, and J. T. Yates, Jr., Surf. Sci. 49, 465 (1975), and Phys. Rev. Lett. 32, 777 (1974).

[4]J. I. Gersten, R. Janow, and N. Tzoar, Phys. Rev. B 11, 1267 (1975).

[5]We have used the Herman-Skillman wave functions to calculate a rough estimate for these potentials.

[6]E. W. Plummer and A. E. Bell, J. Vac. Sci. Technol. 9, 583 (1972); F. M. Propst and T. C. Spicer, J. Vac. Sci. Technol. 4, 53 (1967).

[7]M. A. Van Hove and S. Y. Tong, Phys. Rev. Lett. 35, 1092 (1975).

[8]We use the bond length determined in Ref. 8.

Surface Science 69 (1977) 253–272
© North-Holland Publishing Company

KINETIC THEORY DESCRIPTION OF ELECTRON STIMULATED DESORPTION

Richard JANOW and Narkis TZOAR

Department of Physics, The City College of the City University of New York, New York, New York 10031 USA

Received 5 May 1977

A first principles kinetic theory is developed, applicable to angular dependent emission in Electron Stimulated Desorption. Expressions for the ionic and neutral atom ESD cross sections are formulated and applied in a model calculation of O^+ emission from W(111). Strong focussing of the outgoing ions was found, with the use of a model ion–solid potential in which the substrate was free of excitation. Off-axis spot groups were simulated. The peak ion energies obtained with this model are, however, small compared to experimental energies for the high coverage case. The need to introduce substrate excitations to describe this case is discussed.

1. Introduction

Much work has been done in recent years on the phenomenon of Electron Stimulated Desorption (ESD). In these experiments, a beam of low energy electrons, in the range of 100–500 eV impinges on an adsorbate covered surface, causing the ejection of ions or neutral particles. Several articles reviewing ESD have appeared [1–4].

Experimental data have been collected about the ion yields and cross sections. Energy distributions of emerging ions have been measured [5]. In the last several years, the angular distribution of ejected ions has been investigated [6–8]. Strong focussing of the desorbing ions has been revealed. Desorption patterns were obtained which contain sets of well defined cones for ion emission, both normal and non-normal to the surface. The number and orientation of emission cones is related to the substrate geometry.

ESD Ion Angular Distributions may thus provide valuable clues to the adsorption geometry, on the scale of the unit cell size. This direct information is complementary to that obtained, for example, by LEED, which is sensitive to mainly long range order in the adsorbed layer and substrate.

* Research Sponsored in part by the US Office of Naval Research under ONR contract. No. N00014-75-C-0949 and in part by the City University Faculty Research Award Program.

In this theoretical work, we address ourselves primarily to the angular dependence problem. Previous theoretical treatments of ESD have been strictly one-dimensional, and phenomenological in flavor [9,10]. This work presents a first principles transport formulation of the desorbing ion dynamics. The ion–solid interactions are assumed to be time independent, or long lived relative to ion flight times.

Section 2 establishes the conceptual framework and introduces kinetic equations which can be solved formally, in three dimensions, for the linear response to external electron bombardment. In section 3, expressions for the ionic and neutral atom ESD cross sections are obtained from the kinetic theory, in a form suitable to efficient numerical integration. Section 4 is an illustrative model calculation of ESD Ion Angular Distributions. The experimentally interesting case of O^+ desorption from W(111) was chosen, with the surface assumed free of excitation during the ion ejection. Section 5 is reserved for discussion.

We found that ion interactions with a ground state surface can replicate the focussing and ion distributions in experimental ESD patterns, for several adsorption geometries. However, this model surface potential probably cannot explain the large O^+ ion energies observed at high coverage. We speculatively suggest that long lived excitations on the surface may play the dominent role in ESD of O^+ at high coverage.

2. Formulation of the problem

This calculation employs a multi-step picture of the desorption process which has been found useful in previous ESD investigations [1–4,9–11]. Adsorbed particles are Franck–Condon excited to an anti-bonding state from which ionic desorption may occur. Propagation follows, with the dynamics determined by an effective adparticle–surface interaction potential. Recapture may occur via bond healing transitions. Reneutralized particles may still possess sufficient kinetic energy to escape as neutrals, in which case ground state propagation completes the desorption process.

The above picture is useful for describing the response of adparticle substrate systems which are interacting weakly with an external beam. Hence, we linearize the kinetic equations presented below in the incident flux. Adparticle propagation is described classically. The excitation and decay mechanisms involve electronic transitions, and thus require quantum mechanical descriptions.

A single atom or molecule interacting with a surface may be described by the following Hamiltonian:

$$H = -\frac{\nabla_r^2}{2M} + H_e(r, n_i). \tag{1}$$

Here, H_e contains all the potentials in the system, as well as kinetic energy opera-

tors for electrons which participate in atom--surface interactions. The kinetic energy operator shown acts on adparticle mass center coordinates, with M denoting the adparticle mass.

In the Born–Oppenheimer approximation, the propagation phase of desorption decouples, to order m_e/M, from the electronic states of the system. Electronic responses to shifts in the adparticle coordinates may be regarded as instantaneous, permitting a set of effective interaction potentials to be defined. Excitation and reneutralization are likewise regarded as sudden, inelastic events in which the internal adparticle state, and thus the propagation dynamics, change discontinuously. We assume that the asymptotically recognizable adparticle states partially diagonalize H_e close to the surface.

For the present, consideration is restricted to a two level system, with $n = 1$ for the neutral ground state. For positive ions, $n = 2$. The z-dependent behavior of the

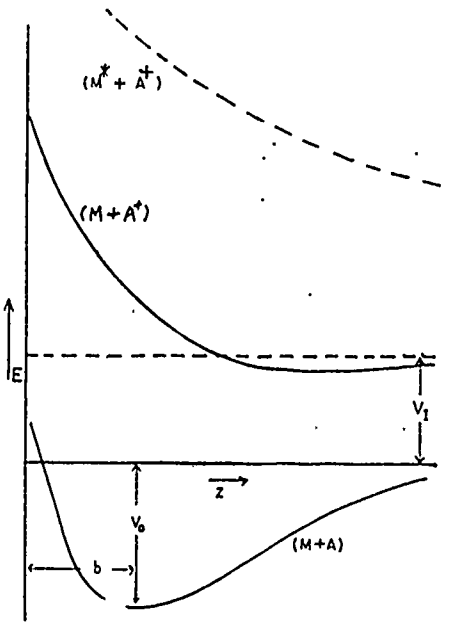

Fig. 1. The one-dimensional qualitative behavior of effective potentials for ionic ESD, as functions of z coordinate. V_0 is the chemisorption energy. The z coordinate of the adsorption site is b. The metal + adsorbate system in its ground state, designated by (M + A), has the potential function $E_1(r)$. An anti-bonding potential $E_2(r)$ leading to ionic ESD is denoted (M + A+). The substrate here is free of excitation. The dashed line M* + A+) suggests the behavior of the effective potential for an ion interacting with the excited substrate. The asymptotic energy difference $E_2 - E_1$ is V_1, the atomic ionization potential, if both incident and ejected electrons are Auger emitted to the vacuum.

effective potentials $E_n(r)$ is sketched qualitatively in fig. 1. The minimum of $E_1(r)$ lies at the chemisorption site. In order for ionic desorption to occur, the antibonding curve $E_2(r)$ must have the generally repulsive character shown. One expects E_2 to become attractive at long range due to image charge density residing on the surface. The difference $[E_2(r) - E_1(r_1)]$ is regarded as the internal ionization energy of the adsorbate. At large adsorbate to surface separations it is identical to the free atomic value. Variations of $E_n(r)$ in the plane parallel to the surface are crucial for the angular dependent desorption problem, and are discussed below.

This picture of desorption, and the transport theory developed below, may be readily generalized to include multiple excited state systems, in which substrate excitations and neutral excited states of adparticles must be considered. In addition, photodesorption may be treated within basically the same formalism [12].

Little attention in the literature has been given to the ionic states which govern the desorption kinetics. Most work has focussed on the ground state potential minima, where adsorption occurs. Studies of electron dissociation of molecules furnish a guide to the antibonding states, however, the model adopted for E_2 in this preliminary study is likely to be crude. The difficulties involved in modelling E_2 for positively ionized cores, are less formidable than for neutrals or negative ions, for which exchange and correlation effects may be important.

The functions $E_n(r)$ are assumed known in developing a kinetic theory below. Furthermore, the solutions of the classical equations of motion for ions and neutral particles are assumed to be known, and to adequately describe propagation of the massive adparticles. The classical solutions $r_n(t)$ depend parametrically on time and on the initial coordinates for each adparticle trajectory.

This classical description is most applicable to unbound, and hence desorbing states. Ions in state 2 quickly acquire substantial kinetic energy. The same argument applies to atoms desorbing in the ground state after suffering reneutralization. A classical description is also acceptable for vibrational states of massive adatoms at high temperatures, that is, when $\hbar\omega_0 \ll kT$. Here, $\hbar\omega_0$ may be taken to be the level spacing for a harmonic oscillator approximation to E_1 near the chemisorption site.

When $\hbar\omega_0 \gtrsim kT$, classical kinetic equations still provide qualitatively correct results for the linear response. The propagation of particles only in unbound trajectories need be followed. The principal correction introduced by quantizing the vibrational states is to modify the shape of ion energy distributions.

We denote by $R(r)$, $Q(r)$ the transition rates for ionization and reneutralization respectively. These functions, assumed known, of adatom-coordinate r are averaged over all initial and final states of the substrate and incident electron consistent with a change of adatom state. Inasmuch as the dominant impulse to adsorbed or desorbing particles is provided in this picture by the gradients of E_n, the small recoil suffered during ionization or non-radiative decay will be neglected.

Electronic energies generally employed in ESD experiments lie in the range 100–500 eV. So long as incident electrons are of high but non-relativistic energy, the excitation phase of ESD may be described in the Born Approximation. For

simple ionization processes, the coordinates of two final state electrons are averaged over in $R(r)$. These exit quickly from the surface region, and are either absorbed by the solid or emitted as Auger electrons to the vacuum. Inasmuch as incident electron energies are large compared to $(E_2 - E_1)$, ionization can occur from within the entire Franck–Condon region.

Non-radiative decay channels dominate transitions back to the ground or low lying excited states. Optical decays are discounted, as their lifetimes are long compared to typical ionic flight times. Ion reneutralization involves matrix elements for electron capture from the solid. Hence, this process is efficient at close range, and weakens rapidly with increasing distance from the surface.

The surface plane is assumed to be tessellated by a periodic grid of of surface unit cells, each of which is anisotropic in the x–y direction. We regard this structure as known. Facetting of the surface, or rearrangements of the substrate layer spacing, which are known to occur under certain conditions, can be incorporated into later calculations as required.

The symmetry and periodicity of the surface mesh are imposed on the functions E_n, R, Q which describe the stages of desorption. Transverse anisotropies in the adparticle–surface interactions become neglible while the atom to surface separation is small compared to the sample dimensions.

We formulate a classical transport theory entirely within a single surface unit cell, extended in the z direction normal to the surface. At macroscopic distances, each such cell behaves as a point source of angular dependent intensity. Transport equations linear in the excitation rate $R(r)$ are now obtained. The rate $Q(r)$ is treated as a zero order quantity. Later calculations verify that the desorption cross sections depend exponentially on $Q(r)$.

Let $P_n(r,v,t)\,\mathrm{d}^3r\,\mathrm{d}^3v$ be the probability of finding an atom or ion in state n at time t, within the phase space volume element at r, v, where these are the ionic position and velocity. The following normalization is assumed, for the present:

$$\sum_{n=1,2} \int_{\substack{\text{unit}\\ \text{cell}}} \mathrm{d}^3r\,\mathrm{d}^3v\,P_n(r,v,t) = 1\,.$$

This condition is relaxed after linearizing the theory.

All spontaneous desorption processes are neglected for the systems we consider at the experimentally interesting temperatures. Thermal desorption may occur as a by-product of local surface heating by the incident electron beam. This effect may be disregarded for weak fluxes.

In the absence of external perturbation, the atom–surface system is taken to be a gas of non-interacting particles in thermal equilibrium with the solid. State 2 is unpopulated, hence:

$$P_2^0(r,v) \approx 0\,.$$

Henceforth, zero superscripts denote equilibrium state quantities. The Boltzmann

equation which describes the ground state is:

$$\upsilon \cdot \nabla_r P_1^0 - \frac{1}{M} \nabla_r E_1 \cdot \nabla_\upsilon P_1^0 = \left(\frac{\mathrm{d}P_1}{\mathrm{d}t}\right)_{\mathrm{SURF}} \approx 0 . \tag{2}$$

Here, M is the adsorbate mass. The surface interaction term describes collisions between adsorbate atoms and substrate excitations. In the present case, these provide principally a relaxation mechanism for the ground state.

Now we allow the system to be driven off equilibrium by an external electron beam. Competition between the relevent transition mechanisms is summarized in the following kinetic equations:

$$\frac{\partial P_2}{\partial t} + \upsilon \cdot \nabla_r P_2 - \frac{1}{M} \nabla_r E_2 \cdot \nabla_\upsilon P_2 = \left(\frac{\mathrm{d}P_2}{\mathrm{d}t}\right)_{\mathrm{E}} + \left(\frac{\mathrm{d}P_2}{\mathrm{d}t}\right)_{\mathrm{Q}} ,$$

$$\frac{\partial P_1}{\partial t} + \upsilon \cdot \nabla_r P_1 - \frac{1}{M} \nabla_r E_1 \cdot \nabla_\upsilon P_1 = \left(\frac{\mathrm{d}P_1}{\mathrm{d}t}\right)_{\mathrm{SURF}} + \left(\frac{\mathrm{d}P_1}{\mathrm{d}t}\right)_{\mathrm{E}} + \left(\frac{\mathrm{d}P_1}{\mathrm{d}t}\right)_{\mathrm{Q}} .$$

Here, the subscripts Q, E refer to the quenching, excitation mechanisms. We made the choice $(\mathrm{d}P_2/\mathrm{d}t)_{\mathrm{SURF}} \approx 0$, in writing the above, thus neglecting scattering and energy loss of the desorbing ions due to interaction with substrate excitations. Such processes will be studied in future investigations.

Ions entering state 2 are described by the source term $(\mathrm{d}P_2/\mathrm{d}t)_{\mathrm{E}}$. Inasmuch as recoil is neglected, one may approximate:

$$(\mathrm{d}P_2/\mathrm{d}t)_{\mathrm{E}} \approx P_1(r, \upsilon, t)\, R(t) ,$$

The corresponding ground state depletion occurring via the ionization process is given by:

$$(\mathrm{d}P_1/\mathrm{d}t)_{\mathrm{E}} = -P_1(r, \upsilon, t)\, R(r) \approx -(\mathrm{d}P_2/\mathrm{d}t)_{\mathrm{E}} .$$

Depletion of the ionic state through reneutralization is given by:

$$(\mathrm{d}P_2/\mathrm{d}t)_{\mathrm{Q}} = -P_2(r, \upsilon, t)\, Q(r)$$

Reneutralized adparticles which re-enter the ground state are the only ones which can desorb in state 1. These contribute a distinctly non-thermal component to P_1, which must be proportional to the following repopulation term, neglecting the recoil upon quenching:

$$(\mathrm{d}P_1/\mathrm{d}t)_{\mathrm{Q}} \approx P_2(r, \upsilon, t)\, Q(r) \approx -(\mathrm{d}P_2/\mathrm{d}t)_{\mathrm{Q}}$$

The following set of kinetic equations, linear in R, describes the angular dependent ESD problem for the weakly perturbed case:

$$\frac{\partial P_2'}{\partial t} + \upsilon \cdot \nabla_r P_2' - \frac{1}{M} \nabla_r E_2 \cdot \nabla_\upsilon P_2' = P_1{}^0 R - P_2' Q , \tag{3a}$$

$$\frac{\partial P_1'}{\partial t} + v \cdot \nabla_r P_1' - \frac{1}{M} \nabla_r E_1 \cdot \nabla_v P_1' = P_2' Q . \tag{3b}$$

All terms here are of order R^1, as required. One-dimensional analogs of eqs. (3a, 3b) were employed in previous work on photodesorption.

In obtaining the result above, we recalled that $P_2^0 \approx 0$. Hence, to lowest order $P_2 \approx P_2' \propto R$. The ground state distribution was taken to be:

$$P_1 = P_1^D + P_1' ,$$

where the depleted equilibrium component P_1^D is defined to satisfy:

$$\frac{\partial P_1^D}{\partial t} + v \cdot \nabla_r P_1^D - \frac{1}{M} \nabla_r E_1 \cdot \nabla_v P_1^D = \left(\frac{dP_1}{dt}\right)_{SURF} - P_1 R .$$

The remaining contribution, P_1', is then the solution to eq. (3b). Inasmuch as P_1^D satisfies an equation independent of Q, a complete description of ground state desorption is yielded by P_1'. Eq. (2) was used to approximate $P_1^D \approx P_1^0$ to dominent order in R. For weak coupling to the electron flux, the characteristic survival time in the ground state against ionization is long compared to the time for substrate induced relaxation. The following condition then holds:

$$(dP_1/dt)_{SURF} \gg (dP_1/dt)_E .$$

Depletion of P_1^0 may then be neglected, as its effect on P_2' and P_1' is of order R^2 at least.

In experimental situations, one ideally observes the current of ions or neutral atoms ejected in each state. Linearity of ESD ion currents with the incident electron flux has been supported by observation. Hence, the intermediate and strong coupling limits of this theory appear to be of little practical interest at present.

3. Desorption cross sections

The total cross section for desorption in the nth state is given by:

$$\sigma_n = I_n(L, t)/F\,\Theta(t) .$$

Here, $I_n(z,t)$ is the net adparticle current in state n crossing a plane parallel to the surface at z, at time t, per unit cell. I_n is evaluated for L large compared to unit cell dimensions. I_n is proportional to both the electron flux F, and to $\Theta(t)$, the number of adsorbed atoms per unit cell remaining on the surface at t. The cross sections are independent of F for linear response. The coverage $\Theta(t)$ and current $I_n(L,t)$ have the same time dependence via $e^{-F\sigma t}$; hence, σ_n is time independent as well. Here σ is the desorption cross section summed over all channels, while t is the elapsed time.

For angular dependent ESD studies. the differential desorption currents $I_n(\theta, \varphi,$

t), and the differential cross sections $\sigma_n(\theta, \phi)$ are of interest. Here θ, ϕ specify the asymptotic emission directions. The asymptotic speeds are integrated over. The total and differential cross sections are related by;

$$\sigma_n = \int d\Omega\, \sigma_n(\theta, \phi) .$$

One may find explicit expressions for $\sigma_n(\theta, \phi)$ in terms of the distribution functions by straightforwardly following the microscopic adparticle flux within one unit cell:

$$\sigma_n(\theta, \phi) = \frac{1}{F} \int_0^\infty d\upsilon\, \upsilon^3 \int_{A_c} d^2 r_\parallel\, P_n(r_\parallel, z = L, \upsilon) .$$

Here $r_\parallel$ lies in the plane parallel to the surface. A_c is the unit cell area. One first evaluates the current density contribution from $d^3\upsilon$:

$$J_n(r, \upsilon, t)\, d^3\upsilon = \Theta(t)\, P_n(r, \upsilon)\, \upsilon d^3\upsilon ,$$

associated with the phase point r, υ.

In view of the complexities associated with the angular dependence problem, we adopt an approach well suited to numerical simulation of ESD Ion Angular Distributions. The explicit result above for the differential cross sections is cumbersome to implement efficiently on the computer.

The steady state ESD response is found by solving an equivalent time dependent problem. We simulate the flux of ions or neutral atoms desorbed in response to an incident electron pulse of short duration τ, then take the limit $\tau \to 0$. Suitable expressions for the total desorption cross sections are constructed using the transport formulation. Numerical differentiation in the asymptotic plane allows one to recover the angular dependence.

This strategy is implemented using the time ordered picture of ESD. An ensemble of adsorbed ground state atoms is perturbed at $t = 0$ by the electron beam. The forward evolution of the system is followed, without further interaction with the external beam, to a time t, when all ions or reneutralized atoms which can desorb have crossed a detection plane. Each trajectory must be individually followed to its asymptotic direction via the classical equations of motion. One evaluates the contribution made by each ion or atom to the cross section, including attenuation due to quenching.

Time dependent solutions of the kinetic equations are required. The formal solutions for P_n map the evolution of an initial distribution function forward in time. These are used to construct the desorption cross sections.

By convention, the dependence of all quantities on r, υ, is suppressed, with only their parametric time dependence displayed. The classical dynamics problem will be solved numerically. Liouvilles Theorem prompts the replacement in eqs. (3a), (3b):

$$\partial/\partial t + \upsilon \cdot \nabla_r + a \cdot \nabla_\upsilon \to d/dt .$$

Here, a is the acceleration in the nth state given by:

$$a = -\frac{1}{M} \nabla_r E_n(r) .$$

Eqs. (3a), (3b) now take the form:

$$dP_2^+(t)/dt = P_1^0(t) R(t) - P_2^+(t) Q(t) , \tag{4a}$$

$$dP_1^+/dt = P_2^+(t) Q(t) . \tag{4b}$$

First, the ionic survival probability against reneutralization, $S_2(t_0, t)$, is defined to be:

$$S_2(t_0, t) \equiv \exp\left[-\int_{t_0}^{t} dt' Q(t')\right] . \tag{5}$$

The exponent is the reneutralization rate integrated along the ionic trajectory from $r(t_0)$ to $r(t)$, which is governed by $E_2(r)$. An alternative notation which displays the path integration explicitly is:

$$S_2(r_0, r) = \exp\left[-\int_{r_0}^{r} \frac{Q(r')v(r')}{|v(r')|^2} \cdot dr'\right]$$

Here, $v(r')$ is the ionic velocity at r'.

It is useful to interpret $S_2(t_0, t)$ as an evolution operator, which maps ions from their initial to final coordinates. One obtains the form of eq. (5) by solving eq. (4a) with the ionization term neglected.

ESD cross sections are experimentally found to be several orders of magnitude smaller than atomic or molecular ionization cross sections would indicate. Hence, quenching is presumed to be efficient and we expect $S_2(t_0, t) \ll 1$, when $r(t_0)$ is close to the surface, and $r(t)$ lies in the detection plane. It is also clear that $S_2(t_0, t)\, S_2(t, t') = S_2(t_0, t')$, and $S_2(t_0, t) = S_2^{-1}(t, t_0)$.

The following trial solution for $P_2^+(t)$ is adopted:

$$P_2^+(t) \equiv g(t)\, S_2(t_0, t) .$$

After formally differentiating the above and comparing with eq. (4a) the unknown function g(t) is found to satisfy:

$$dg(t')/dt' = R(t')\, P_1^0(t')\, S_2^{-1}(t_0, t') .$$

The formal solution $P_2^+(t)$ for the ionic state is

$$P_2^+(t) = P_2^+(t_0) S_2(t_0, t) + P_1^0(t_0) \int_{t_0}^{t} dt' R(t') S_2(t', t) . \tag{6a}$$

Here, we integrated the equation for $g(t)$ formally over $t_0 \leqslant t' \leqslant t$. The boundary

condition $g(t_0) = P_2'(t_0)$ is found by taking the limit $t \to t_0 + \epsilon$. One notes that $\lim_{t \to t_0} S_2(t_0, t) = 1$.

Both $R(t)$, $Q(t)$ are assumed to be mathematically well behaved. The equilibrium distribution satisfied $P_1^0(t) = P_1^0(t_0)$.

The solution $P_2'(t)$ yields the ionic distribution function which has evolved from the initial distributions $P_2'(t_0)$ and $P_1^0(t_0)$. The first term in eq. (6a) attenuates the initial ion density, while the second incorporates ionizations which occur during the interval $[t_0, t]$.

The formal solution of eq. (4a), containing the ground state component of quenched particles, is:

$$P_1'(t) = P_1'(t_0) + \int_{t_0}^{t} dt' \, P_2'(t') \, Q(t') . \tag{6b}$$

Here, one uses the state 1 dynamics to map $r(t)$, $v(t')$ forward to time t in the second term.

We construct the cross sections after first examining the response of a single ground state adatom to ionizing transitions during the short finite interval $[-\tau, 0]$. Let $U^+(-\tau, 0)$ be the probability of finding the atom as an ion at $t = 0$. Using eq. (6a) this is found to be:

$$U^+(-\tau, 0) = \int_{-\tau}^{0} dt' \, R(t') \, S_2(t', 0) . \tag{7}$$

Here, the choice $P_2'(-\tau) = 0$ was made, inasmuch as the initial ionic population must be excluded from the response during $[-\tau, 0]$. We normalized to unit source strength with the choice $P_1^0(t_0) = 1$. The explicit value of U^+ is fixed by the choice of initial conditions $r(-\tau)$, $v(-\tau)$.

Next, a single ion is permitted to evolve from $t = 0$ to time t, when its velocity has reached the asymptotic value. No further interaction with the external electrons is included; hence, we choose $P_1^0(t_0 = 0) = 0$, and $P_2'(t_0 = 0) = 1$ in eqs. (6a), (6b). Conditional probabilities for finding the atom with $r(t)$, $v(t)$ are given by:

$$V^+(0, t) = S_2(0, t)$$

for the ionic state, and

$$V^0(0, t) = \int_{0}^{t} dt' \, S_2(0, t') \, Q(t')$$

for the ground state. An ion may reneutralize at any time after $t = 0$. Hence, $V^0(0, t)$ contains an integration over intermediate times.

The single atom ejection probabilities, $T^{+,0}(-\tau, 0, t)$, for the ionic and neutral state, follow the history of an adsorbed atom which responds to the external beam over $[-\tau, 0]$:

$$T^{+}(-\tau, 0, t) = U^{+}(-\tau, 0)\, V^{+}(0, t), \quad T^{0}(-\tau, 0, t) = U^{+}(-\tau, 0)\, V^{0}(0, t). \tag{8}$$

These quantities are closely related to the ionic and neutral atom desorption cross sections to be presented below.

Let $\chi_\epsilon(r_0)$ denote the ionization cross section for an adsorbed atom at the point $r_0 = r(t = 0)$. This function must have the free atomic or molecular ionization cross section as its limit when $z_0 \to \infty$. Here, ϵ is the incident electron energy. We expect $\chi_\epsilon(r_0)$ to be linear in the upward transition rate R_ϵ as follows:

$$\chi_\epsilon(r_0) = R_\epsilon(r_0)/F \tag{9}$$

Here, F is the incident electron flux.

This result is recovered after first noting that $U^{+}(-\tau, 0)/\tau$ is the average ionization rate per atom. The corresponding average ionization cross section per atom is given by:

$$\bar{\chi}_\epsilon(-\tau, 0) = \frac{1}{F\tau} \int_{-\tau}^{0} dt'\, R_\epsilon(t')\, S_2(t', 0).$$

In the limit $\tau \to 0^{+}$ one obtains the instantaneous response. $R_\epsilon(t')$ is smoothly varying for ESD, inasmuch as the summations over final state electron coordinates contained in R consume any delta function resonances. One factors $R_\epsilon(t' = 0)$ from the integration above, and makes the replacement $S_2(t', 0) \approx S_2(-\eta, 0) = 1$ to obtain eq. (9).

The cross section for the entire process resulting in ionic desorption of an atom initially in the ground state is given by:

$$\sigma^{+}_{EJ}(0, t) = \chi_\epsilon(r_0)\, V^{+}(0, t)$$

$$= \frac{R_\epsilon(r_0)}{F}\, \Theta\left(\tfrac{1}{2}Mv_0^2 + E_2(r_0) - E_2(\infty)\right) \exp\left[-\int_0^t dt' Q(t')\right].$$

Here, the dependence on R and Q is displayed. The step function was inserted to ensure that desorption is energetically possible. One integrates the decay probability appearing in the exponent from point to point as the trajectory is followed. The asymptotic velocity generated by σ^{+}_{EJ} depends on the choice of r_0, v_0. One chooses t for each ion path so that $z(t)$ lies far from the surface.

The analogous ground state ejection cross section is given by:

$$\sigma^{0}_{EJ}(0, t) = \chi_\epsilon(r_0)\, V^{0}(0, t) = \chi_\epsilon(r_0) \int_0^t dt' Q(t') \exp\left[-\int_0^{t'} dt'' Q(t'')\right]$$

$$\times\, \Theta\left[\tfrac{1}{2}Mv_0^2 + E_2(r_0) - E_2(r') + E_1(r') - E_1(\infty)\right].$$

Here, the step function was evaluated at the reneutralization point, eliminating trapped particles. E_2 governs the path integrations during $[0, t']$, while E_1 determines the dynamics during $[t', t]$. Numerical evaluation of σ^0_{ij} is expected to be time consuming due to the integration on intermediate times.

Finally, the ensemble averages of ejection cross sections over the phase space coordinates is taken at $t = 0$. The formal solutions which yield the total ionic and neutral atom ESD cross sections are:

$$\sigma_c^+ = \int d^3r_0\, d^3v_0\, P_1^0(r_0, v_0)\, \chi_c(r_0)\, S_2(0, t)\, \Theta[\tfrac{1}{2}Mv_0^2 + E_2(r_0) - E_2(\infty)], \tag{10a}$$

$$\sigma_c^0 = \int d^3r_0\, d^3v_0\, P_1^0(r_0, v_0)\, \chi_c(r_0) \int_0^t dt'\, S_2(0, t')\, Q(t')$$

$$\times\, \Theta[\tfrac{1}{2}Mv_0^2 + E_2(r_0) - E_2(r') + E_1(r') - E_1(\infty)]\,. \tag{10b}$$

The equilibrium distribution P_1^0 was used in averaging, rather than P_1, inasmuch as the ejection cross sections are already linear in R. Eq. (10a) for σ^+ is employed below in the numerical simulation of ESDIAD for O^+ adsorbed on tungsten.

Note that eq. (10a) for σ^+ is a generalization of phenomenological expressions which have appeared in the literature. Our previous work on one dimensional photodesorption theory produced expressions analogous to Eqns (10a, 10b) for the optically fluorescent and ground state cross sections.

The result expressed in eqs. (10a), (10b) is model independent, except for general restrictions on R, Q, E_m, and P_1^0 outlined above. One may use eqs. (10a), (10b) in conjunction with model surface interactions to obtain ESDIAD patterns and energy spectra within the Menzel--Gomer, Redhead ESD picture.

Finally, note that the transport approach is applicable to a wide variety of surface phenomena involving propagation of atoms, ions or molecules. In particular, the cross section contributions due to higher order excitation processes in ESD may be obtained without difficulty.

4. Model calculation for O^+ desorption from tungsten

The remainder of this paper applies the first principles kinetic theory in a model calculation of desorption from tungsten. We attempt to understand the interesting angular and energy dependent ESD results found recently on W(111) [6] by numerically simulating the ESD patterns and ion energy spectra to be expected for atoms adsorbed at various sites on the surface. Little is known of the nature of possible antibonding states for ions; therefore, simple models are adopted for ion–solid and atom–solid interactions. Absolute cross sections were not calculated due to

lack of information about wave functions on surfaces. We concentrate on the spectroscopy of ESD; that is, in this paper we have studied only the polar and azimuthal angular dependence and the energy spectra of emerging ions.

Experimentally, a rich diversity of ESDIAD patterns were found on W(111) and W(100). For high coverage, these consist of groups of sharp O^+ emission spots, whose geometry is a function of adsorption and annealing temperature. O^+ emission normal to the surface was found, as well as off normal spots, whose number and orientation clearly reflect the underlying substrate geometry.

The antibonding state potential funnel is assumed to be the mechanism which produces focussed spot patterns. For a number of the observed ESDIADs, one can discount the possibility that off axis emission is due to thermally activated substrate facetting [13]. Here, only flat substrates are considered.

The peaks in ion energy spectra were found to occur at 8 to 9 eV, on both W(100) and W(111) [6–8]. This agrees with earlier studies [5] on polycrystalline tungsten which report a spectrum peaking at 8.8 eV.

The qualitative features of our result are unaltered by the following choice of models. Spacial variation in the excitation and reneutralization rates was neglected; thus, we chose χ_c and S_2 to be constants. When vibrational states are highly localized, the distortion of σ^+ introduced by this approximation is not critical. Ion energy spectra will be skewed toward lower energies, as the preferential reneutralization of slower ions is neglected.

Near a possible adsorption site, we modelled E_1 as a parabolic potential:

$$E_1(r) \approx -V_0 + \tfrac{1}{2}(r - b)\, K(r - b).$$

Here, b is the adsorption site coordinate. The chemisorption energy V_0 does not appear explicitly in these calculations. The spring constant tensor K was taken to be isotropic, for simplicity. One fits $K_{\alpha\beta}$ to the best experimental values.

We chose for P_1^0 gaussian distributions both in position and velocity spaces. This choice is appropriate for particles in an harmonic potential well both for high temperature, and in the zero temperature case. The shape of ion energy spectra results from a folding of P_1^0 against E_2 in these calculations. However, peak ion energies are insensitive to the width of P_1^0. This sixfold integration on phase coordinates r_0, v_0 in eq. (10a) was accomplished by the Monte Carlo method.

In modelling E_2, ions were approximated as point charges which respond to the local electrostatic surface potential. The character of the dominent anti-bonding state in ESD is not known: for simplicity, we chose to examine one which leaves the substrate free of excitation. E_2 is taken to be the sum of the unexcited substrate Hartree potential, plus an image contribution, produced by averaged electron density fluctuations, viz:

$$E_2(r) \approx q\, V_{\mathrm{IM}}(r) + q \sum_{R_j} V_{\mathrm{A}}(r - R_j).$$

Here, q is the ionic charge. Bonding effects in the substrate were neglected. The sur-

face Hartree potential was represented by the sum of free tungsten atom Hartree potentials centered on the lattice sites. Similar superpositions have been the starting point for self-consistent band structure calculations in bulk tungsten [14–16].

The Herman–Skillman wave functions [17] were used to evaluate V_A numerically, which was then fitted to the form:

$$V_A(r) \approx 7.72\, e^{-1.29r}.$$

All quantities are in atomic units. As a check, we evaluated also the screened tungsten atomic potential in the Fermi–Thomas approximation. At realistic $W-O^+$ separations, the resulting potential is somewhat smaller than the above,

An ion–surface plasmon hamiltonian [18,19] was used to numerically evaluate the image potential V_{IM}, for a number of values of z and r_s, the plasma parameter. The result for singly ionized atoms was fitted, to the following form:

$$V_{IM}(z, r_s) \approx -1/[4z + 1.16 + 1.34\, r_s + O(r_s^2)] .$$

Image charge density resides, in this model, on an approximate electronic boundary of the metal. Including plasmon dispersion shifts the divergence in the classical result at the dielectric surface to the interior of the metal.

Some consequences of this ESD model on W(111) are now examined. Extensive numerical computation using 100 K for the desorption temperature was done, at a wide variety of possible adsorption sites.

The most striking result follows: the naive model constructed for the anti-bonding potential strongly focusses ions created in the neighborhood of most plausible candidates for adsorption sites. The most compact simulated O^+ emission spots are associated with the largest mean ion energies. Long range image attraction tends to defocus the spots. However, this mechanism is competitive with focussing by the repulsive component of E_2 only for very low energy ions.

Each adsorption site candidate produces a single emission spot. For higher energy ions, the local value of $-\nabla E_2$ at the point of ionization provides the dominent impulse, and sets both the central colatitude and azimuthal orientation relative to the substrate for the resulting emission spot. In many cases, the dominent contribution to E_2 comes from a single substrate atom. Emission spot geometry then reflects the chemisorption bond direction.

We were successful in generating simulated ion distributions quite similar to those which were observed on W(111). Success, however, in replicating the visual features of ion distributions does not guarantee that this model for the antibonding state is applicable. In particular, the simulated ion energy spectra which were produced peak well below the experimental ion energies. This was the case even for adsorption site candidates whose ESDIAD pattern simulations closely resemble those observed. This finding is discussed further in the concluding section. For now, we remark that remodeling of the anti-bonding state is required.

Despite the limitations of this model, it is useful to explore the most plausible

picture of high coverage oxygen chemisorption it can generate, guided by experiment.

Whenever the anti-bonding state potential has the qualitative behavior of our model, the following rules associate the gross features of ESDIAD spot patterns with adsorption geometry. Emission spots directed off the surface normal are evidence of adsorption at a point where E_2 is assymmetric, that is, away from the one fold degenerate unit cell sites. Here, we define n fold degeneracy to mean that a particular point is found in n equivalent locations within a single unit cell whose environments are identical except for combinations of rotation, reflection, and translation. For example, in fig. 2 all the points labelled $\alpha, \beta, \gamma, \delta$ are degenerate. At

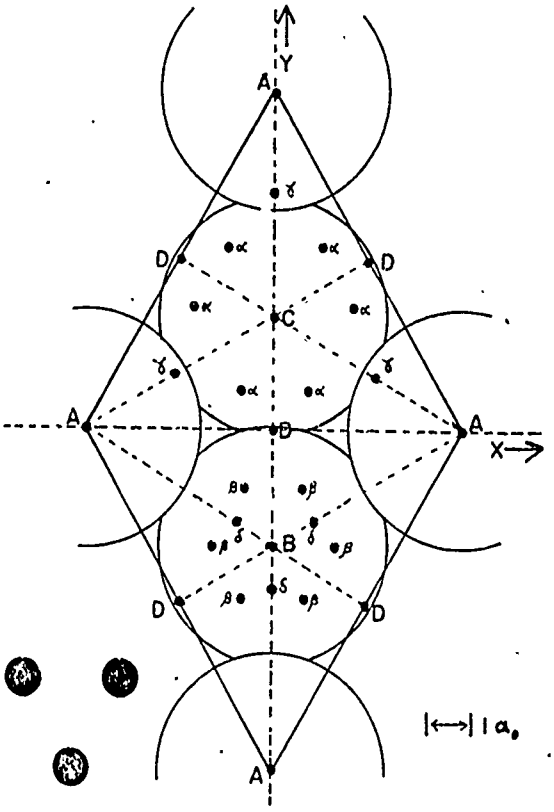

Fig. 2. The W(111) surface unit cell. Large spheres depict tungsten atoms. The A atoms lie in the surface layer. B and C atoms reside in the second and third planes in the solid. The A–A distance is 8.44 a_0. Dashed lines through B, C are bilateral symmetry axes. "Primary" ESD emission lobes for O^+ on W(111) have been observed, with their substrate registry as indicated by the trio of heavy circles.

the high symmetry (onefold degenerate) sites, the anti-bonding potential possesses approximate azimuthal symmetry, and thus leads to emission peaked normal to the surface.

One would reconsider this interpretation if long lived, highly localized substrate excitations could be shown to dominate in the anti-bonding potential. Such excitations might be localized on neighboring adsorbate or substrate atoms, and could result in non-normal emission of atoms adsorbed at symmetric points.

Within the model we used, symmetrical groupings of off axis spots are explained. Assymmetric points in the unit cell are several-fold degenerate. An adsorbate domain on the surface in which such sites are occupied should be found, with equal occupation probability, in all degenerate orientations. The corresponding ESDIAD patterns should thus contain spot superpositions suggestive of the substrate unit cell structure.

We illustrate with applications of the model to W(111). Fig. 2 shows the W(111) surface unit cell. Some of the lengths pertinent to the W–O system in are tabulated in table 1. Here we are guided by experiment. Under conditions for which facetting of the surface is believed not to occur, trios of O^+ emission spots were found, having the substrate orientation shown in fig. 2. These were found in conjunction with normal emission, or with a second spot trio, rotated 180°.

In this simulation, adsorption at the highly assymmetric points such as α or β in

Table 1
Some characteristic lengths in the tungsten–oxygen system; unless noted otherwise, lengths are taken from either Slater [20] or Pauling [21]

Empirical atomic radii (Å)		
Oxygen	[20]	0.60
	[21]	0.66
Tungsten	[20]	1.35
	[21]	1.30
Bulk tungsten (bcc) lengths (Å)		
Lattice constant		3.16
W–W interatomic spacing		2.74
W(111) surface lengths (Å)		
Lattice constant		4.47
Interplanar spacing		0.91
W(100) surface lengths (Å)		
Lattice constant		3.16
Interplanar spacing		1.58
W–O bond lengths (Å)		
Sum of empirical atomic radii	[20]	1.95
	[21]	1.96
Experimental W–O bond length on W(111) [22]		2.08 ± 0.07

fig. 2 can produce only patterns of six spots, rotated from the observed orientation. Adsorption directly over one of the highly symmetric points A, B, or C produces only emission in a narrow cone normal to the surface. Adsorption elsewhere along the unit cell mirror planes is expected to generate spot trios, with primary oriented spots, as in fig. 2, corresponding to adsorption between points A and C, while 180° rotated trios correspond to occupied sites between C and B, or B and A.

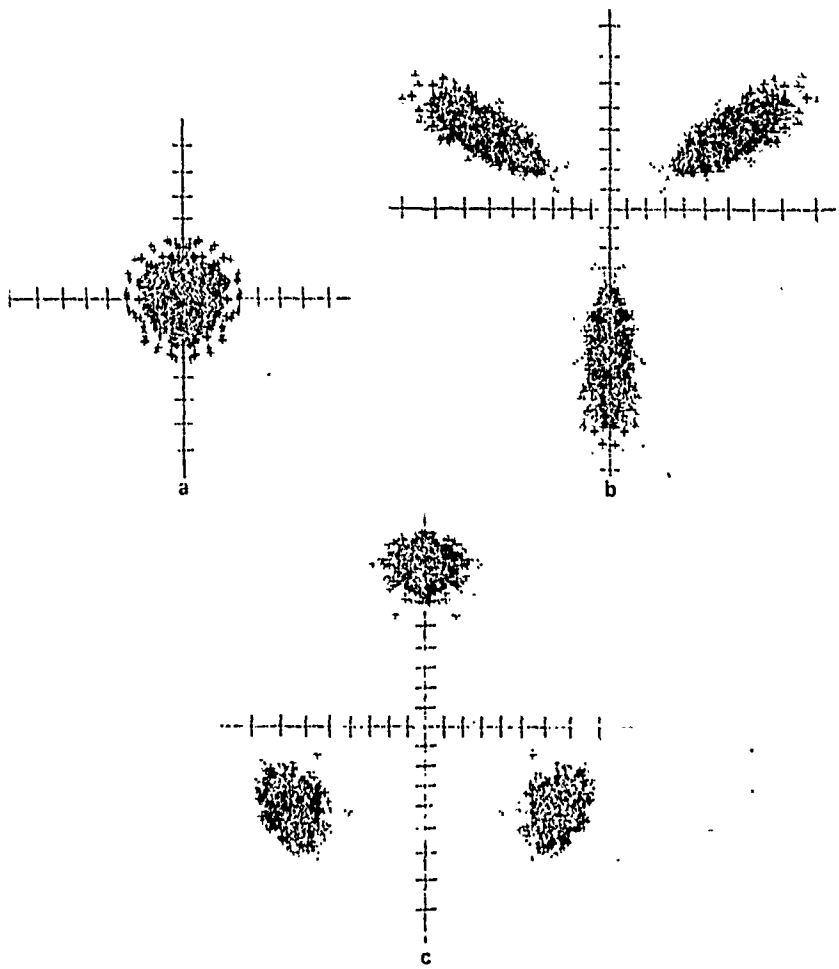

Fig. 3. Simulated ESD spot patterns for low coverage of oxygen on W(111). (a) shows the ion distributions for adsorption 1.95 Å, over point C on fig. 2; (b) corresponds to adsorption almost equidistant from tungsten atoms at A and C; while (c) pertains to adsorption between sites C and B. This series provides the best fit to experimental patterns of Madey et al. Scale marks correspond to 5° increments in asymptotic colatitude θ. The projection $x = \tan\theta \cos\phi$, $y = \tan\theta \sin\phi$ was used.

We located those sites which yield the best fit with this anti-bonding potential, to the experimental ESDIAD patterns and ion energies. A reasonable lower limit on the W–O bond length was chosen as 1.95 Å, the sum of Slater's atomic radii [20–22]. The colatitude of simulated primary lobes was fitted to the experimental [6] value of 34°.

The most plausible site candidate found for the origin of 'primary' spot trios (i.e., those with the orientation shown in fig. 2) lies almost equidistant from the A and C layer tungsten atoms, in fig. 2, along the unit cell mirror plane. A site almost equidistant from the C and B layer tungsten atoms is this models best choice for the generator of 180° rotated spot trios.

For both of these sites, the mean energy of emitted ions was calculated to lie in the range 2 to 2.5 eV, which is significantly smaller than the experimental value of 8–9 eV. For the normal emission spot produced by adsorption directly over point C, this model predicts ions energies peaking at 1.3 eV. Note that these calculations predict peak ion energies an order of magnitude below experiment, for adsorption sites directly above the surface layer tungsten atoms at A. Fig. 3 shows the spot patterns for sites mentioned.

5. Discussion, conclusions

The first principles kinetic theory presented above for angular dependence in ESD provides a vehicle for testing model ion-solid interactions. Calculations performed using a simple model for the ground state surface anti-bonding potential predict strong focussing of ions, like that observed in ESDIAD experiments involving O^+ emission. Models of O^+ chemisorption on W were inferred, by fitting to the experimental patterns. Unfortunately, poor agreement between our calculated ion energy distributions and the experimental [5] ones weakens the plausibility of such chemisorption models, for high oxygen coverage on tungsten. However, we expect these model calculations to apply to low oxygen coverage on W for which O_2 is believed to dissociate. It is likely at low coverage, that the metallic substrate will support only excitations whose lifetimes are much shorter than ion ejection times.

Complementary model calculations for O^+ desorption from W(100) were done. Some of the results have been reported in the literature [11]. Here, we remark that the ion energy distributions obtained in model computations peak at about 2.5 eV, as for W(111).

Substantially the same picture of adsorption results from a range of models for the antibonding potentials which are time independent, and which involve basically scale and range changes. More careful modelling of the potential for ground state surfaces may moderately increase the calculated ion energies. For example, we replaced the tungsten wave function by a set which includes L–S coupling [23], then repeated calculations for some selected sites. Ion energies were increased by a factor of roughly 1.5 to 2, with neglible change in the simulated ESDIAD patterns.

It appears unlikely, however, that a model anti-bonding state in which the substrate and remaining adsorbate atoms are free of excitation can adequately explain the high ion energies observed for β_1 oxygen.

It is interesting to note that ion energy spectra peaking at 1.7 eV. were reported for ESD of H^+ from tungsten [5]. This is consistent with the energy range predicted by our model.

We speculatively suggest that excited antibonding states involving the surface and adsorbate atoms may be able to explain the large O^+ ejection energies found at high coverage. Explicit detailed treatment of these as yet unknown states requires cluster calculations beyond the scope of this work.

The type of processes we suggest are analogous to those involved in electron dissociation of free molecules. A collision with an incident electron leaves the local surface in a state from which an adsorbate ion dissociates. The local region is left as an excited fragment, which produces the antibonding effective potential governing ion propagation. Excited states may be distributed over an extended cluster, or localized to one or several neighboring atoms.

Surface excitations can produce ion energies in the range observed for O^+ on W, provided their lifetime is long compared to times spent near the surface by ions. Picture a simplistic process, for example, which leaves both O^+ and W^+ on the surface. The coulomb interaction, at 1.95 Å separation, yields 7–8 eV energies. For O_2 molecules, energies are ~12 eV.

In this picture, the lifetimes of surface excitation must be long compared to ionic flight times. Otherwise, the strong anti-bonding potential shuts off immediately after its creation, leaving the ground state surface potential to provide the dominent impulse to desorbing ions, as in the model calculations presented above. Long lifetimes for surface excitations may be justified if one postulates a transition in surface behavior from metallic to insulating, as coverage approaches a full monolayer for oxygen. Note that the experimental O^+ energies pertain to the high coverage β_1 phase.

Insight into the physical reasons for a low yield β_2 and a high yield β_1 oxygen phase can be gained, if this insulating barrier picture is a realistic one for high coverage. In addition to supporting long lived excitations, such a barrier would inhibit ion reneutralization. Both higher ion energies and smaller hopping matrix elements would appear in the reneutralization rate, compared to a low coverage surface. Dramatic increases in the ion survival probability would result, due to the exponential dependence of S_2 on $Q(r)$.

ESD emission of H^+ from W can probably be explained using the ground state surface model, with no need to postulate the formation of an insulating barrier at high coverage. The H^+ yield for both β_1 and β_2 hydrogen phases is small, and comparable to that of oxygen in the low coverage phase.

We can devise speculative mechanisms which produce geometrical spot patterns in ESDIADs, whether it is the ground state surface potential or an excited antibonding state which governs ion emission. If the anti-binding state is associated

with highly localized excitations, off axis spots can result even in the case where adsorption occurs at the highly symmetric points of the unit cell. Note, for example, on fig. 2, that an adsorbate ion created above point C, together with excitation of an adjacent A layer tungsten atom, can produce downward facing spot trios. If excited states are multi-centered, the anti-bonding potential will have essentially the same symmetry as the ground state potential. Off-axis spot groups then correspond to adsorption at points in the unit cell away from the symmetry sites.

The speculative nature of some of our remarks indicates the need for accelerated theoretical study of ESD mechanisms, after which unambiguous adsorption site determinations using ESDIAD may be made.

References

[1] R. Gomer, Solid State Phys. 30 (1975) 94.
[2] D. Menzel, Surface Sci. 47 (1975) 370.
[3] T.E. Madey and J.T. Yates, Jr., J. Vacuum Sci. Technol. 8 (1971) 525.
[4] J.H. Leck and B.P. Stimpson, J. Vacuum Sci. Technol. 9 (1972) 273.
[5] M. Nishijima and F.M. Propst, Phys. Rev. B2 (1970) 2368.
[6] T.E. Madey, J. Czyzewski and J.T. Yates, Jr., Surface Sci. 57 (1976) 580.
[7] J. Czyzewski, T.E. Madey and J.T. Yates, Jr., Phys. Rev. Letters 32 (1974) 777.
[8] T.E. Madey, J. Czyzewski and J.T. Yates, Jr., Surface Sci. 49 (1975) 465.
[9] D. Menzel and R. Gomer, J. Chem. Phys. 41 (1964) 3311, 3329.
[10] P.A. Redhead, Can. J. Phys. 42 (1964) 886.
[11] J. Gersten, R. Janow and N. Tzoar, Phys. Rev. Letters 36 (1976) 610.
[12] J. Gersten, R. Janow and N. Tzoar, Phys. Rev. B11 (1975) 1267.
[13] J.C. Tracy and J.M. Blakely, Surface Sci. 13 (1968) 313.
[14] J.O. Dimmock, Solid State Phys. 26 (1971) 103.
[15] L.F. Matheiss, Phys. Rev. 139 (1965) A1893.
[16] T.L. Loucks, Phys. Rev. 143 (1966) 506.
[17] F. Herman and S. Skillman, Atomic Structure Calculations (Prentice Hall, 1965).
[18] N. Tzoar and J. Gersten, Phys. Rev. B8 (1973) 5671, 5684.
[19] J. Gersten and N. Tzoar, Phys. Rev. B9 (1974) 4038.
[20] J.C. Slater, Quantum Theory of Molecules and Solids, Vol. II (McGraw-Hill, 1965).
[21] L. Pauling, The Nature of the Chemical Bond, 3rd ed. (Cornell Univ. Press, 1960).
[22] M. Van Hove and S. Tong, Phys. Rev. Letters 36 (1975) 1092.
[23] D. Liberman, J. Waber and D. Cromer, Phys. Rev. 137 (1965) A27.

Relation between electron-stimulated desorption and nondissociative chemisorption*

Joel I. Gersten and Narkis Tzoar
Department of Physics, City College of the City University of New York, New York, New York 10031
(Received 18 November 1976; revised manuscript received 10 February 1977)

A relation is found between the maximum ion energy associated with electron-stimulated desorption (ESD) and the chemisorption bond length. This relation suggests that the large kinetic energy of the desorbed ion may be understood in terms of ESD of undissociated molecules.

The phenomenon of electron-stimulated desorption (ESD) of ions from solid-state surfaces has been a topic of considerable interest within the last decade.[1,2] The adatom-substrate system is assumed to be promoted by the incident electron to a repulsive energy curve resulting in the ejection of an ion from the surface. The ions are emitted with a rather broad energy distribution extending up to some maximum energy E_{max}. In this paper we will show how important information concerning the chemisorption bond may be obtained from a knowledge of E_{max}.

We shall be concerned with molecular gases absorbed on various substrates. For some systems it is believed that the molecule chemisorbs as a unit, while for other systems there is evidence that dissociation occurs, and that the chemisorbed species is atomic, at least at low coverages. Most of the experimental information concerning ESD which we shall discuss comes from high-coverage conditions, where the bonding situation is not that well understood.

In order to interpret E_{max}, one must have an insight into the nature of the repulsive states involved in ESD. Before considering the case of a molecule absorbed on a surface, consider the simpler problem of dissociative ionization of gaseous H_2. In the electron-impact event, both of the molecular electrons may be regarded as being excited to higher orbitals. There is clearly a rich abundance of excited states available culminating in those states where the molecule is left doubly ionized. In most of the excited states the electronic wave function expands to a size where it is no longer effective in screening the internuclear repulsion. If s denotes the bond length, one expects E_{max} to be roughly given by

$$E_{max} = e^2/S\,, \tag{1}$$

where E_{max} represents the upper limit to the kinetic energy available to the dissociating atoms.

The situation for more complicated diatomic molecules cannot be radically different. While it is possible to excite the more tightly bound orbitals, the cross section for such a process will be negligibly small compared with that for disruption of the highest-lying orbital pair. Thus one expects Eq. (1) to remain valid.

In the case of a free molecule, the repulsive energy is partitioned between the dissociating particles in a manner consistent with energy and momentum conservation. When the molecule is absorbed on a surface, the situation is more complicated. Let us invoke a model where one ion desorbs, whereas its partner atom (or ion) remains bound to the surface. It is convenient, but not necessary, to think of this binding as being harmonic in nature. As the ion desorbs, the bound atom-solid system may be left in any of the excited vibrational states. It is important to realize, however, that there is a finite probability of being left in the ground state, i.e., that *recoilless desorption* may occur. This implies that the maximum energy available to the desorbing ion is, in fact, still given by Eq. (1). There is no recoil correction that has to be made to this energy.

There is some indirect evidence, in fact, that this is the case. If one studies the energy distribution of the emitted ions as a function of the primary electron energy (Lozier plot) near the threshold, one experimentally finds a slope of unity.[3] The interpretation given [3] is that the mass of the recoiling complex is very large, but it is clear that it could also be interpreted as a manifestation of recoilless desorption.[4]

In Table I we have assembled experimental data for various molecules absorbed on several substrates. The molecular bond lengths S_1 were obtained from gas-phase data.[5] We have also included an estimate of the atom-substrate bond length, S_2, by averaging the homonuclear diatomic bond lengths.[6] If the molecule remains undissociated, then e^2/S_1 is the appropriate value for E_{max}, whereas if it does dissociate, it is likely that e^2/S_2 is the correct value (assuming that the substrate atom can become singly ionized).

Comparison of the theoretical predictions with the experimental values for E_{max} suggest that in most cases quoted here the results may be under-

TABLE I. Comparison of theory and experiment.

Molecule	Substrate	Reference	E_{max} (eV)	S_1 (a_0)	S_2 (a_0)	e^2/S_1 (eV)	e^2/S_2 (eV)	Dissociated?
O_2	W	7	13	2.28	3.9	11.9	7.0	No
		8	12.5					
O_2	Mo	1	11.3	2.28	3.72	11.9	7.3	Both
		8	7.5					
O_2	Ni(110)	8	11	2.28	3.50	11.9	7.7	No
O_2	Si(111)	9	11.3	2.28	3.3[illegible]	11.9	8.1	No
O_2	Ge(111)	9	11.6	2.28	3.46	11.9	7.9	No
CO	W	7	12	2.13	3.9	12.8	7.0	No
CO	Graphite	10	12.2	2.13	2.13	12.8	12.8	No
H_2	W	7	7	1.40	3.[illegible]	19.4	8.3	Yes
NO	W	11	11.2	2.18	3.9	12.5	7.0	No
H_2O	W	7	15	1.81	3.3	15.0	8.3	No
CO_2	W	7	10	2.53	3.9	10.8	7.0	No

stood in terms of ESD due to undissociated molecules. Exceptions to this occur for H_2 on tungsten, where reasonable agreement with experiment is obtained for the dissociation model. The case of O_2 on Mo is interesting because it appears to exhibit both dissociated and undissociated molecules under different experimental conditions.

The model presented here is extremely simple. It neglects effects due to image forces and residual surface fields. The fact that the model works so well can be taken as evidence that these effects are not important. This is consistent with the fact that the surface is strongly oxidized in the high-coverage phases of chemisorption.

In the present discussion we are neglecting the smearing of the high-energy cutoff due to the zero-point fluctuations in the position of the ground state adatom. This will be small due to the slow spatial variation of the Coulomb potential. The full width at half maximum for this is estimated to be $\Delta E = (\mu\omega s^4/\ln 16)^{1/2}$, where μ is the reduced mass of the adatom, and ω is the vibrational frequency of the undissociated molecule. For CO and O_2, for example, ΔE is 0.9 eV.

*Research supported by the Office of Naval Research under Contract No. N00014-75-C-0949.

[1]P. A. Redhead, Can. J. Phys. 42, 886 (1964); D. Menzel and R. Gomer, J. Chem. Phys. 41, 3311 (1964).

[2]For an extensive review of the early literature, see T. E. Madey and J. T. Yates, Jr., J. Vac. Sci. Technol. 8, 525 (1971).

[3]P. A. Redhead, Nuovo Cimento Suppl. 5, 587 (1967); J. W. Coburn, Surf. Sci. 11, 61 (1968).

[4]Note that if one considers the atom-solid system, the phenomenon is very similar to the Mössbauer effect.

[5]G. Hertzberg, *Spectra of Diatomic Molecules*, 2nd ed. (Van Nostrand, Princeton, 1967).

[6]*Handbook of Chemistry and Physics*, 47th ed., edited by R. C. Weast (Chemical Rubber Co., Cleveland, 1967).

[7]M. Nishijima and F. M. Propst, Phys. Rev. B 2, 2368 (1970).

[8]H. H. Madden, J. Vac. Sci. and Technol. 13, 228 (1976).

[9]M. I. Datsiev, Zh. Tekh. Fiz. 39, 1284 (1969) [Sov. Phys.-Tech. Phys. 14, 965 (1970)].

[10]M. I. Datsiev and Yu.I. Belyakov, Zh. Tekh. Fiz. 38, 742 (1968) [Sov. Phys.-Tech. Phys. 13, 554 (1968)].

[11]J. T. Yates, Jr., T. E. Madey, and J. K. Payn, Nuovo Cimento Suppl. 5, 558 (1967).

Surface Science 75 (1978) L766–L772
©North-Holland Publishing Company

LETTER TO THE EDITOR

CALCULATION OF ENERGY SPECTRA FOR ESD OF H^+ FROM H_2 ADSORBED ON TUNGSTEN *

Received 1 December 1977; manuscript received in final form 3 March 1978

Electron Stimulated Desorption is a phenomenon in which a beam of low energy electrons (100–500 eV) impinges on an adsorbate covered surface, causing the ejection of ions or neutral particles. Ion yields, ESD total cross sections, and energy distributions have been found experimentally for a variety of adsorbate–substrate combinations. Most recently, angular dependent patterns of strongly focussed ion impact spots have been observed, whose geometry may reflect the substrate unit cell structure [1–3]. ESD data provide important clues to the chemisorption geometry and insight into the character of surface interactions. Several recent review articles exist [4–7].

A phenomenological model of the ESD process in one dimension was suggested [8,9] by Gomer, Menzel and Redhead (GMR). This multistep model pictures absorbate atoms to be promoted via Franck–Condon transitions from a bound vibrational level to an excited anti-bonding state, which may dissociate with the emission of an ion.

This paper presents a first principles calculation of the kinetic energy distribution for H^+ ions desorbed from tungsten surfaces via ESD. Here we amplify previous work, which focussed primarily on the angular dependence in O^+ emission [10, 11]. A kinetic theory applying to ESD in three dimensions was formulated in our earlier work from first principles using a generalization of the GMR picture. Ions were assumed to move classically, with their dynamics governed by an adparticle–surface effective potential Bond healing reneutralization mechanisms may cause ions to be recaptured. These may desorb as neutrals, if their history as ions provides sufficient kinetic energy. The electronic transitions involved in ionization and quenching (reneutralization) necessitate quantum mechanical descriptions of these processes.

This study of H_2/W is prompted by our recent findings for O^+ desorbed from O_2/W. We calculated ESD Ion Angular Distributions and energy spectra, using simple models for the interaction of O^+ with the surface. Despite the crudity of the model potential employed, rough agreement of calculated peak ion energies with

* Research Sponsored by the US office of Naval Research under ONR constract No. N00014-75-C-0949.

4

experiment should have been obtained, if a ground state surface generates the potential relevent to emission dynamics.

Experimental determination of the β_1 state (high coverage) O^+ energy peak yields 8.8 eV, and a large spectral width which constrasts sharply with the prediction of our model for O^+. Strong focussing effects and the main features observed in ESDIAD's were, however, replicated in our earlier work for several speculative oxygen adsorption geometries. We are currently investigating the hypothesis that either molecular absorption or long lived excited states on the surface may explain the ESD spectrum of O^+.

Note that the experimental energy distribution for ESD of H^+ from H_2/W peaks at 1.7 eV for high coverage on polycrystalline material [12]. This lies in the range expected with a ground state surface model. Attention is therefore restricted here to calculating the H^+ spectrum, inasmuch as it provides a critical test of the GMR picture of ESD employed in previous work. The detailed calculations closely parallel those discussed in ref. [10]. Reasonable values were adopted for some of the phenomenological parameters required.

A three-dimensional model for the anti-bonding H^+–W surface potential was constructed for W(100), W(111), and W(110), in the manner described in earlier work [10]. Here H^+ ions are assumed to respond to a time independent potential field which we approximate by the sum of unperturbed tungsten atom Hartree potentials, plus an image contribution. The corresponding force governs ionic motion following dissociation from the surface.

Experimental evidence indicates that H_2 adsorbs on W in atomic form – with recent experimental confirmation. At high coverage (≈2 atoms/unit cell) the characteristic vibration energy is 135 MeV, contrasting sharply with that expected for molecular vibrations.

We approximated the ground state potential for hydrogen atoms by three-dimensional parabolic wells at each of several test adsorption sites, using spring constants matched to the experimentally determined vibration frequencies.

At 300 K, the ground state vibration level spacing is large compared to the thermal energy. Hence, absorbed hydrogen atoms are assumed to vibrate in the zero point harmonic oscillator state. H atoms ionized by electron impact are represented by a minimum uncertaintly wave packet corresponding to a classical Gaussian distribution of the form:

$$P_1^0(r, v) = \prod_{l=1}^{3} \{(2\pi\rho_l\nu_l)^{-1} \exp(-v_l^2/2\nu_l^2) \exp[-(r_l - b_l)^2/2\rho_l^2]\} . \quad (1)$$

Here b locates the adsorption sites. The widths in atomic units are given by

$$\rho_l = (2m\omega_l)^{-1/2} , \quad \nu_l = (\omega_l/2m)^{1/2} . \quad (2)$$

The parameters used in this calculation yield $\rho_l \approx 0.24\, a_0$. The finite width in velocity space was included but has negligible effect.

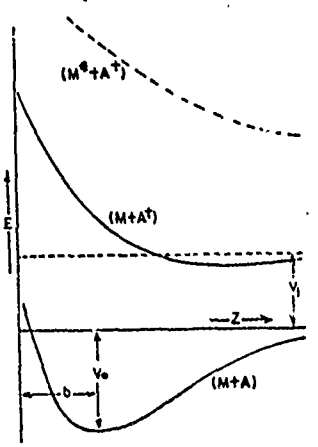

Fig. 1. The qualitative behavior of the effective potentials for ionic ESD, as functions of the z coordinate. V_0 is the chemisorption energy. The z coordinate of the adsorption site is b. The metal + adsorbate system in its ground state is designated by (M + A). An anti-bonding potential leading to ionic ESD is denoted ($M + A^+$). The substrate here is free of excitation. The dashed line ($M^* + A^+$) suggests the behavior of the effective potential for an ion interacting with the excited substrate. The asymptotic energy difference is V_1, the atomic ionization potential, if both incident and ejected electrons are Auger emitted to the vacuum.

We limited our calculation to the shape of ion energy distributions, which are obtained by folding the ion–solid potential E_2 against the ground state distribution. Fig. 1 provides a one-dimensional illustration, with gaussian shape of P_1^0 skewed to form a high energy tail in the spectrum, due to variation in the slope of E_2. The spectral shape will also be modulated by the ion survival probability against reneutralization. In the present calculation, reneutralization effects are taken to be independent of initial position, as is the ionization cross section. The parameters required to construct realistic models of reneutralization are not yet known.

This (GMR) interpretation of kinetic energy spectra is a good description of ESD only if the substrate remains in its ground state during ion propagation, which is assumed here, or if the potential is produced by substrate excitations whose lifetimes are long compared to ion flight times. If the cross section to produce surface excitations is large enough, with the decay lifetime comparable to the time of flight, another width mechanism may contribute via competition between the relaxation and reneutralization lifetimes. Inelastic recoil involving substrate and adsorbate atoms may also widen the ion spectra. This mechanism, however, should not be significant for light ions.

It was necessary to calculate H^+ desorption spectra for each of the W(100), W(111), and W(110) faces, inasmuch as the polycrystalline sample used by Nishijima and Propst [12] had an unknown mixture of faces. We calculate spectra for hydrogen atoms adsorbed at each of several highly symmetric points on each unit

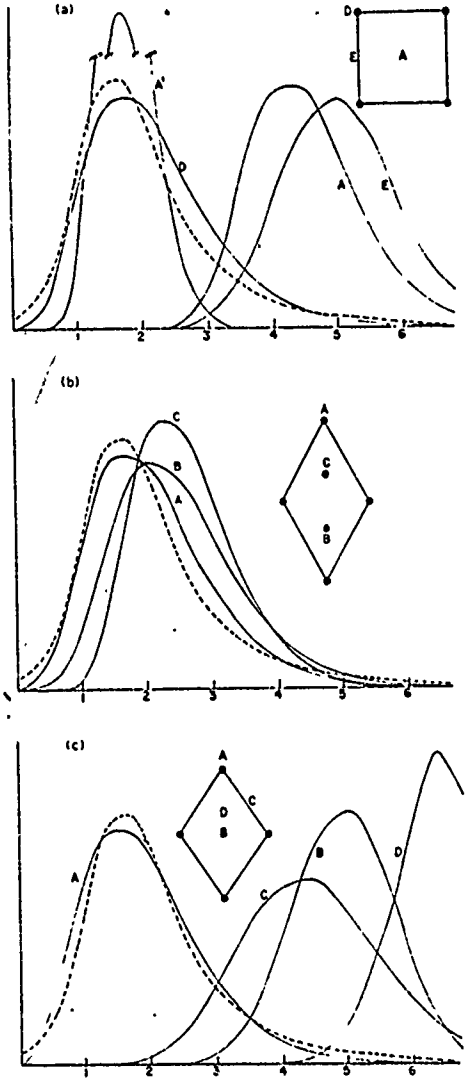

Fig. 2. (a), (b) and (c): calculated ion energy distributions for ESD of H^+ from H_2 on W(100), W(111), and W(110). All spectra are normalized to unity, with energies given in electron volts. The broken curve shows experimental results of Nishijima and Propst [12]. On each surface, highly symmetric sites were chosen for calculation, as shown by the Insets for each surface geometry, with $3.3\,a_0$ taken to be the W–H bond length. On W(100), site A′ is five-fold coordinated, site E is a two-fold coordinated bridge site, and sites A, D are singly coordinated. On W(111), all sites are singly coordinated $3.3\,a_0$ above W atoms. On W(110), sites B, C are bridge sites, site D is three-fold coordinated to surface layer W atoms and site A is singly coordinated over the surface.

surface cell. Experimental ESDIAD spot patterns for H^+ on W(100) support this symmetric choice of sites [2].

Fig. 2 summarizes numerical results for each of the tungsten faces studied. For comparison, we have plotted the H^+ experimental spectrum normalized to the same scale. The low energy portion of this spectrum appears gaussian, while above the peak at 1.7 eV one finds a tail, having an algebraic appearance, and an apparent cut-off at about 7 eV. It is interesting to point out that the experimental spectrum for O^+ desorption from W, in particular, as well as those for some other systems studied experimentally peak at significantly higher energies, and do not display a pronounced tail.

On each surface studied, we find calculated spectra which closely mimic the experimental one in width, peak ion energy, and in the presence of a tail.

The best agreement on each face is found for the hydrogen adsorption sites directly over a surface layer tungsten atom. We speculate that these may have filled in the high coverage situation which produced the experimental results.

Note that the five-fold coordinated site A′ on W(100) also produces a spectrum peaking near 1.7 eV. This, however, is sharply peaked, exhibiting no significant trace of a tail. Site A′ has been suggested for the low coverage β_2 phase of H_2/W(100). Several mechanisms discussed below might contribute to broadening the spectrum.

Reneutralization is a strong process in this system, as evidenced by the small ESD cross section for H^+, and by the known large magnitude of isotope effects. Depending on realistic values of several parameters, reneutralization may cause broadening and skewing of the spectra in fig. 2 to either higher or lower energy. The one-dimensional limit of our kinetic theory, together with a simple model, furnishes an illustration.

First impose a Born–Mayer form for the H^+–W potential:

$$E(z) = V_0 \exp[-\alpha(z - b)]. \tag{3}$$

For the H^+ reneutralization rate we assume:

$$Q(z) = Q_0 \exp[-\beta(z - b)]. \tag{4}$$

Here b is the chemisorption site coordinate.

Apart from a normalization constant, the resulting spectrum [12] is

$$F(\epsilon) \propto \epsilon^{-1} \exp[-\tfrac{1}{2}(\ln \epsilon/x)^2] \exp\left[-\frac{Q_0}{\alpha}\left(\frac{m\pi}{2V_0}\right)^{1/2}\left(\frac{\Gamma(R)}{\Gamma(R+\frac{1}{2})}\right)\epsilon^{R-1/2}\right]. \tag{5}$$

Here, $\epsilon = E/V_0$ and $x = \alpha/(2m\omega)^{1/2}$, all in atomic units. The second exponential expresses modulation of the spectrum due to quenching, with the ratio $R = \beta/\alpha$ of the ranges providing a measure of competing effects associated with quenching. It is reasonable to expect R of order unity, since the range of both Q and E depend on the tails of wave functions of the solid which extend into the vacuum.

A priori, fast ions might be assumed to have the lowest probability to be reneu-

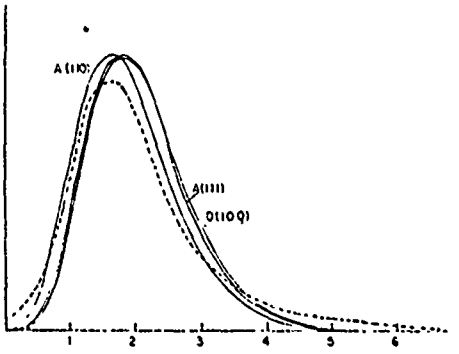

Fig. 3. Calculated spectra for ESD of D^+ from tungsten. Here, spectra for the sites directly over surface tungsten atoms are shown.

tralized. On the other hand, fast ions are those created closest to the surface, and which interact most strongly with substrate electrons increasing the quenching probability. The sense in which the resulting energy spectrum is skewed is strongly model dependent. For $R = 1/2$, quenching is uniform but for $R > 1/2$ the relative intensity of spectral tails present in fig. 2 sould be reduced. The opposite effect occurs for long range quenching, defined here by validity of the condition $R > 1/2$.

Experimental ESD spectra for D^+ from D_2/W might be useful in establishing reneutralization effects, due to mass dependence in the exponent above. The vibrational states, however, possess complicating mass dependence. The prominent tails in some of the calculated H^+ spectra in fig. 3 can be attributed to the large amplitude of zero point motion for light particles. Fig. 3 shows calculated D^+ spectra, which show considerable narrowing compared to their counterparts in fig. 2.

Note that higher order processes which involve surface excitations are possible contributors to the H^+ spectrum in the region near its cutoff above 7 eV. The limiting energy is given by the H^+–W^+ Coulomb repulsion, which is about 8 eV for 3.3 a_0 separation. Somewhat lower energies are expected for high rydberg surface states. Some preliminary calculations, using a delta function model for the vibrational state distribution, show that finite width spectra can be produced via competition between the surface state lifetime and the reneutralization rate. A site such as A′ might produce a broadened spectrum via such processes. Another process possibly contributing to the broadening makes use of coupling between translational states of the ions and vibrations in the surface. Significant energy loss would result from the creation of such multiphonon final states.

To summarize, these results for ESD of H^+ from H_2/W support the theoretical picture of ESD proposed by GMR and formalized in our previous work. Despite the crudity of the models used, this calculation produces energy spectra consistent with experiment for several surfaces and plausible atomic adsorption sites. In par-

ticular, our model H^+–W potential, in which the surface remains free of excitation, provides a qualitatively correct description for ESD of H^+ from H_2/W. The lack of experimental data about ESD cross sections and reneutralization effects prohibits us from making definitive statements which would select the dominant surfaces and adsorption sites contributing to the experimental H^+ spectrum.

Richard JANOW and Narkis TZOAR
Department of Physics, The City College of the City University of New York, New York, New York 10031, USA

References

[1] T.E. Madey, J. Czyzewski and J.T. Yates, Jr., Surface Sci. 57 (1976) 580.
[2] J. Czyzewski, T.E. Madey and J.T. Yates, Jr., Phys. Rev. Letters 32 (1974) 777.
[3] T.E. Madey, J. Czyzewski and J.T. Yates, Jr., Surface Sci. 49 (1975) 465.
[4] R. Gomer, Solid State Phys. 30 (1975) 94.
[5] D. Menzel, Surface Sci. 47 (1975) 370.
[6] T.E. Madey and J.T. Yates, Jr., J. Vacuum Sci. Technol. 8 (1971) 525.
[7] J.H. Leck and B.P. Stimpson, J. Vacuum Sci. Technol. 9 (1972) 273.
[8] D. Menzel and R. Gomer, J. Chem. Phys. 41 (1964) 3311, 3329.
[9] P.A. Redhead, Can. J. Phys. 42 (1964) 886.
[10] R. Janow and N. Tozar, Surface Sci. 69 (1977) 253.
[11] J. Gersten, R. Janow and N. Tzoar, Phys. Rev. Letters 36 (1976) 610.
[12] M. Nishijima and F.M. Propst, Phys. Rev. B2 (1970) 2368.

Surface Science 84 (1979) 440–448
© North-Holland Publishing Company

THE INTERACTION OF POLAR-OPTICAL PHONONS WITH A TWO-DIMENSIONAL ELECTRON GAS *

Narkis TZOAR
Department of Physics, The City College of The City University of New York, New York, New York 10031, USA

Received 15 December 1978; manuscript received in final form 12 February 1979

The interaction Hamiltonian for a two-dimensional electron gas with optical phonons was obtained, for an electron gas on the interface of a polar semiconductor in a metal–insulator–semiconductor device. We found that the electron–phonon interaction is proportional to the inverse square root of the phonon wave number. The dependence of the electron–phonon coupling constant on the dielectric constant of the insulator is determined.

1. Introduction

When an electric field is applied to the surface of a semiconductor, as occurs in metal–insulator–semiconductor devices under bias, a strong accumulation of electrons on the surface of the semiconductor takes place, known as inversion layer. These electrons are trapped by a surface potential and are bound in the direction normal to the surface, but are free to move on the plane defined by the semiconductor–insulator interface. Since the average distance between electrons within the plane is larger than their spread normal to the plane, one may describe the behaviour of the electrons in the inversion layer as two-dimensional.

The study of transport and optical properties of two-dimensional electron gas is an active area of research. In previous work mostly non-polar semiconductors have been considered [1]. Thus electron–impurity, electron–accoustic phonons and multivalleys electron–electron collisions have been studied [2–8]. However, a recent interest in polar semiconductors motivates the present paper [9]. Here an important scattering mechanism results from the interaction of longitudinal polar phonons with the electrons. We present a dielectric formulation [10–12] for the interaction of a two-dimensional electron gas and polar phonons. We derive, using general principles, both the matrix element for the electron–phonon scattering and the surface polar phonon frequencies.

* Research sponsored in part by the US Office of Naval Research under ONR grant No. N00014-75-C-0949 and by The City University Faculty Award Program.

2. Excitations and interactions in semi-infinite dielectric

The long wavelength excitations of a semi-infinite polar crystal can be characterized by a scalar potential. Here we neglect entirely the small region of very long wavelengths, where phase velocities of the excitation roughly equal the speed of light, and retardation effects become important. The excitation spectrum of semi-infinite crystals and their interactions with electrons is describable in terms of the bulk dielectric function $\epsilon(k, \omega)$. We think of these excitations as potential waves propagating in the medium and inducing polarization charges.

We start with the well known case of the infinite crystal. Here the excitation spectrum is given in terms of the longitudinal optical phonons characterized by their wave number k and frequency ω_k. In terms of the destruction (creation) operators b_k ($b_k^\dagger$) the scalar potential is given by

$$\phi = (2\pi)^3 V^{-1} \sum_k M_k b_k \exp(\mathrm{i}k \cdot r - \mathrm{i}\omega_k t) + \text{h.c.} \tag{1}$$

The coefficients M_k are at present arbitrary. In order to connect M_k to the dielectric properties of the crystal, we let a charge travel through the crystal; i.e. the charge density ρ is:

$$\rho = Q\delta(r - vt), \tag{2}$$

and the interaction Hamiltonian has the form:

$$H_{\text{int}} = \int \mathrm{d}r\, \rho\phi = Q(2\pi)^3 V^{-1} \sum_k M_k b_k \exp(\mathrm{i}k \cdot vt - \mathrm{i}\omega_k t) + \text{h.c.} \tag{3}$$

From time-dependent perturbation theory we calculate the transition amplitude to the first order in H_{int}

$$C = (-\mathrm{i}/\hbar) \int_{-\infty}^{+\infty} \mathrm{d}t\, \langle H_{\text{int}} \rangle, \tag{4}$$

where $\langle H_{\text{int}} \rangle$ denotes the matrix element for one phonon emission. Standard calculations leads to the rate of energy loss of the charged particle which is given by:

$$-\mathrm{d}W/\mathrm{d}t = \sum_k \hbar\omega_k (2\pi)^6 V^{-2} (Q^2/\hbar) |M_k|^2 2\pi\, \delta(\omega_k - k \cdot v). \tag{5}$$

So far our expression for the energy loss is exact. Here, however, we intend to calculate M_k, for wavenumbers smaller than the characteristic lattice wave number. We shall do this by comparing a formula for the energy loss obtained by using dielectric (or continuum) formulation with eq. (5). We shall rewrite eq. (5) considering only long wavelength phonons and keeping in mind a cutoff for large wavenumbers. We therefore neglect the dispersion of the phonons, as usual, (i.e. ω_k is replaced by ω_1,

the longitudinal phonon frequency) and obtain

$$-\mathrm{d}W/\mathrm{d}t = (2\pi)^3 V^{-1} \int \mathrm{d}k\, Q^2 |M_k|^2 (2\pi/\hbar)\, \omega_l \delta(\omega_l - k \cdot v), \tag{6}$$

which is the rate of energy loss of the charge Q moving through the crystal.

We shall next take a classical approach and calculate $\mathrm{d}W/\mathrm{d}t$ for a charge Q transversing a dielectric medium. The charge density ρ is given in eq. (2). The potential induced by the charge can be written as

$$\Phi(r, t) = \int \mathrm{d}k\, \mathrm{d}\omega \exp(ik \cdot r - i\omega t)\, \Phi(k, \omega), \tag{7}$$

and similarly the charge density may be written as:

$$\rho(r, t) = \int \mathrm{d}k\, \mathrm{d}\omega \exp(ik \cdot r - i\omega t)\, \rho(k, \omega). \tag{8}$$

From the Poisson equation we have the relation between potential, charge and dielectric function:

$$\Phi(k, \omega) = 4\pi\, \rho(k, \omega)/k^2\, \epsilon(k, \omega), \tag{9}$$

where eqs. (2) and (8) give:

$$\rho(k, \omega) = Q\delta(\omega - k \cdot v)/8\pi^3. \tag{10}$$

Thus, from eqs. (9), (10) and (7), the induced potential is now given by

$$\Phi(r, t) = \int \mathrm{d}k\, \mathrm{d}\omega \exp(ik \cdot r - i\omega t)\, Q\delta(\omega - k \cdot v)/2\pi^2 k^2\, \epsilon(k, \omega), \tag{11}$$

and the electric field is given by $E = -\nabla\Phi$. Following Ritchie [10] the work done on the charge is given by:

$$\frac{\mathrm{d}W}{\mathrm{d}t} = \lim_{r \to vt} Q(E - E_0) \cdot v = \frac{Q^2}{\pi^2} \int \mathrm{d}k \int_0^\infty \mathrm{d}\omega\, \frac{\omega}{k^2} \mathrm{Im}\left[\frac{1}{\epsilon(k, \omega)}\right] \delta(\omega - k \cdot v). \tag{12}$$

Here E_0 is the induced field in vacuum which is obtained upon replacing $\epsilon(k, \omega)$ in eq. (11) by unity. We have also made use of the reality condition $\epsilon^*(k, \omega) = \epsilon(k, -\omega)$.

We next use the long-wavelength limit of the dielectric function of the crystal and approximate

$$\epsilon(k, \omega) \Rightarrow \epsilon(\omega) = \epsilon_\infty (\omega^2 - \omega_t^2)/(\omega^2 - \omega_t^2). \tag{13}$$

Here ω_t is the transverse phonon frequency, and ω has a small positive imaginary constant to ensure that $\epsilon(\omega)$ is the retarded dielectric response. Using eqs. (12) and

(13) we obtain:

$$-\frac{dW}{dt} = \frac{Q^2}{\pi^2}\int dk\, \frac{\omega_l^2 - \omega_t^2}{2\epsilon_\infty k^2}\pi\delta(\omega_l - k\cdot v). \tag{14}$$

Upon comparing eqs. (6) and (14) we obtain [13]

$$|M_k|^2 = \frac{V}{(2\pi)^3}\frac{\hbar\omega_l}{4\pi^2k^2}\left(\frac{1}{\epsilon_\infty} - \frac{1}{\epsilon_0}\right), \tag{15}$$

where ϵ_∞ (ϵ_0) is the high (low) frequency dielectric constant of the solid. This leads to a potential

$$\phi(r, t) = V^{-1/2}\sum_k (-i)\left[\frac{2\pi\hbar\omega_l}{k^2}\left(\frac{1}{\epsilon_\infty} - \frac{1}{\epsilon_0}\right)\right]^{1/2} \times b_k \exp(ik\cdot r - i\omega_l t) + \text{h.c.}, \tag{16}$$

and to an interaction Hamiltonian for the electron–phonon system, given by

$$H_{int} = \int dr\, \rho_e\phi = \int dr\, e\sum_s \delta(r - r_s)\,\phi = V^{-1/2}\sum_s\sum_k (-i)\left[\frac{2\pi e^2}{k^2}\hbar\omega_l\left(\frac{1}{\epsilon_\infty} - \frac{1}{\epsilon_0}\right)\right]^{1/2}$$

$$\times \exp(ik\cdot r_s - i\omega_l t)\, b_k + \text{h.c.}, \tag{17}$$

where r_s represents the electronic coordinates.

For the case of semi-infinite crystal the situation is somewhat more complicated. Here we lose our translational invariance, say, in the z direction. As far as the bulk properties are concerned, the semi-infinite and the infinite crystal are identical. However one should consider here the reflection of the vibrational modes by the surface discontinuity, which leads to slightly different set of eigenfunctions.

We consider the dielectric approach for the polar crystal excitation spectrum and make a Fourier expansion of the electrostatic potential

$$\Phi(r, t) = \int dk\, d\omega \exp(ik\cdot r - i\omega t)\,\Phi(k, \omega). \tag{18}$$

We take the crystal for $z < 0$ and thus for $z > 0$ the Laplace equation demands that

$$\int dk\, d\omega \exp(ik\cdot r - i\omega t)\, k^2\,\Phi(k, \omega) = 0. \tag{19}$$

Hence $k^2\Phi(k, \omega)$ is an analytic function in the upper k_z plane. Inserting this into eq. (18) leads to the result

$$\Phi(r, t) = \int dk_\perp\, d\omega \exp(ik_\perp\cdot r - i\omega t)\, A(k_\perp, \omega)\exp(-k_\perp z), \tag{20}$$

for $z > 0$, where

$$A(k_\perp, \omega) = [(\pi/k_\perp)\, k^2\,\Phi(k, \omega)]_{k_z = ik_\perp}.$$

Here $k_\perp$ is a two-dimensional vector in the x–y plane. The choice of the potential in the crystal $z < 0$ is somewhat arbitrary. However for our purposes we choose the potential to be the sum of two terms. One of them is a reflection of the $z > 0$ potential, which makes Φ continuous across $z = 0$. The second term must vanish at $z = 0$, in order to assure the continuity of Φ across the plane $z = 0$. We thus write

$$\Phi(r, t) = \int \mathrm{d}k_\perp \, \mathrm{d}\omega \int_0^\infty \mathrm{d}k_z \, B(k, \omega) \, \theta(-z) \sin(k_z z) \exp(\mathrm{i}k_\perp \cdot r - \mathrm{i}\omega t)$$

$$+ \int \mathrm{d}k_\perp \, \mathrm{d}\omega \, A(k_\perp, \omega) \exp(-k_\perp |z|) \exp(\mathrm{i}k_\perp \cdot r - \mathrm{i}\omega t), \tag{21}$$

where the integral on k_z was taken from 0 to ∞ to avoid double counting. Here eqs. (20) and (21) represent our general solution for $\Phi(r, t)$, for all space, in the continuum approximation. This potential can be used to describe electron–phonon processes having small momentum transfer, i.e. much smaller than lattice momentum for both bulk and surface electrons.

Using our choice of potential, one may interpret it as having a bulk term that exists for $z < 0$ and vanishes at the surface, and a surface term which exponentially falls towards zero for large values of $|z|$. Thus, as in the case of metal–insulator–semiconductor devices when electrons are trapped in the insulator–semiconductor interface, the electron–phonon interaction depends on the surface term in $\Phi(r, t)$. Also note that the reality of Φ impose symmetry relations on both A and B. We now make contact with the phonon field and express the arbitrary coefficients A and B in terms of the phonon coordinates. Here ω_k as before is the eigenvalue of the bulk phonon having wavenumber k, and $\Omega_{k_\perp}$ is the eigenvalue of the localized surface phonon having wavenumber $k_\perp$. Our potential is now given by:

$$\phi(r, t) = (2\pi)^3 V^{-1} \sum_k [M_k b_k \sin(k_z z) \exp(\mathrm{i}k_\perp \cdot r - \mathrm{i}\omega_k t) \, \theta(-z) + \mathrm{h.c.}]$$

$$+ (2\pi)^2 A^{-1} \sum_k [N_{k_\perp} a_{k_\perp} \exp(-k_\perp |z|) \exp(\mathrm{i}k_\perp \cdot r - \mathrm{i}\Omega_{k_\perp} t) + \mathrm{h.c.}], \tag{22}$$

where b_k ($b_k^\dagger$) is the destruction (creation) operator of the bulk phonon and $a_{k_\perp}$ ($a_{k_\perp}^\dagger$) is the destruction (creation) operator of the surface phonon. The interaction Hamiltonian is given by

$$H_{\mathrm{int}} = \int \rho(r, t) \, \phi(r, t) \, \mathrm{d}r.$$

We are however interested in the surface modes and their coupling to surface electrons and thus choose our ρ to be

$$\rho(r, t) = Q \, \delta(z) \, \delta(r_\perp - v_\perp t), \tag{23}$$

where $r_\perp$ and $v_\perp$ are two-dimensional vectors parallel to the surface. As before we calculate the matrix element $\langle H_{\rm int}\rangle$ between no-phonon and one-surface-phonon states and evaluate the energy loss rate to be:

$$-\frac{dW}{dt} = Q^2 \int dk_\perp\, \Omega_\perp \frac{(2\pi)^3}{\hbar A} |N_{k_\perp}|^2\, \delta(\Omega_\perp - k_\perp \cdot v_\perp). \tag{24}$$

In eq. (24) we have already replaced $\Omega_{k_\perp}$ by $\Omega_\perp$, the long wavelength surface phonon frequency.

We now calculate, using the classical approach, the energy loss of a charge moving on the surface of the crystal. Here rather than solving the potential in the $z<0$ region for the inhomogeneous problem, we wish to consider an infinite crystal. However we must impose an image charge to account for the dielectric discontinuity at $z=0$. We choose an induced surface charge:

$$\rho_s = \delta(z)\, \sigma(r_\perp, t), \tag{25}$$

which together with ρ, eq. (23), and the Poisson equation result in the Fourier transform of the potential;

$$\Phi(k,\omega) = \frac{4\pi}{k^2\, \epsilon(k,\omega)} \left[\frac{Q}{8\pi^3}\delta(\omega - k_\perp \cdot v_\perp) + \frac{\sigma(k_\perp,\omega)}{2\pi}\right], \tag{26}$$

where $\sigma(k_\perp,\omega)$ is the Fourier coefficient of $\sigma(r_\perp, t)$. We therefore obtain for the potential in the $z<0$ region:

$$\Phi(r,t) = \int dk\, d\omega\, \frac{4\pi}{k^2\, \epsilon(k,\omega)} \left[\frac{Q}{8\pi^3}\delta(\omega - k_\perp \cdot v_\perp) + \frac{\sigma(k_\perp,\omega)}{2\pi}\right] \exp(ik\cdot r - i\omega t). \tag{27}$$

For $z>0$ region, the potential is given as before by:

$$\Phi(r,t) = \int dk_\perp\, d\omega\, A(k_\perp,\omega) \exp(-k_\perp z) \exp(ik_\perp \cdot r - i\omega t). \tag{28}$$

We next impose the usual boundary conditions: (i) Φ is continuous across $z=0$ and (ii) the jump in D_z is proportional to the external surface charge density, and obtain the following conditions:

$$[k_\perp/\tilde{\epsilon}(k_\perp,\omega)]A(k_\perp,\omega) = 2\pi\, \sigma(k_\perp,\omega) + (Q/2\pi)\,\delta(\omega - k_\perp\cdot v_\perp),$$
$$\epsilon_b k_\perp A(k_\perp,\omega) = -2\pi\, \sigma(k_\perp,\omega) + (Q/2\pi)\,\delta(\omega - k_\perp \cdot v_\perp). \tag{29}$$

In eq. (29), $\tilde{\epsilon}(k_\perp,\omega)$ is defined by:

$$\tilde{\epsilon}(k_\perp,\omega) = (k_\perp/\pi) \int_{-\infty}^{+\infty} dk_z\, [k^2\, \epsilon(k,\omega)]^{-1}, \tag{30}$$

and ϵ_b is the dielectric constant of the barrier or the oxide. The solution of eq. (29)

yields

$$A(k_\perp, \omega) = \frac{Q}{\pi k_\perp} \frac{\bar{\epsilon}(k_\perp, \omega)}{1 + \bar{\epsilon}(k_\perp, \omega)\epsilon_b} \delta(\omega - k_\perp \cdot v_\perp),$$

$$\sigma(k_\perp, \omega) = \frac{Q}{4\pi^2} \frac{1}{1 + \bar{\epsilon}(k_\perp, \omega)\epsilon_b} \delta(\omega - k_\perp \cdot v_\perp). \tag{31}$$

Our eqs. (27), (28) and (31) constitute the solution of the electrostatic field in the entire region. In order to calculate the energy-rate loss of the charge we need the field when the crystal is replaced by its surrounding "vacuum" which in, our case, is the barrier having dielectric constant ϵ_b. Using eq. (30), $\bar{\epsilon}$ must be replaced by ϵ_b^{-1} and we obtain for $z = 0_+$ that:

$$(E - E_0) \cdot v_\perp = \int dk_\perp \, d\omega \exp(ik_\perp \cdot r - i\omega t) \left(\frac{k_\perp \cdot v_\perp}{i}\right) \frac{Q}{2\pi k_\perp \epsilon_b}$$

$$\times \left[\frac{2\epsilon_b \bar{\epsilon}(k_\perp, \omega)}{\epsilon_b \bar{\epsilon}(k_\perp, \omega) + 1} - 1\right] \delta(\omega - k_\perp \cdot v_\perp). \tag{32}$$

Using the relation $[\bar{\epsilon}(k_\perp, \omega)]^* = \bar{\epsilon}(k_\perp, -\omega)$ the energy-loss rate is given by:

$$-\frac{dW}{dt} = \int dk + \int_0^\infty d\omega \frac{2\omega Q^2}{\pi k_\perp \epsilon_b} \delta(\omega - k_\perp \cdot v_\perp) \operatorname{Im}\left(\frac{1}{\bar{\epsilon}(k_\perp, \omega) + \epsilon_b^{-1}}\right). \tag{33}$$

We next approximate $\epsilon(k, \omega)$ by its local (spatially) approximation for long wavelength excitation, i.e.

$$\epsilon(k, \omega) \cong \epsilon_\infty \frac{\omega^2 - \omega_l^2}{\omega^2 - \omega_t^2}.$$

Using eq. (30) we obtain

$$\bar{\epsilon}(\omega) = \frac{1}{\epsilon_\infty} \frac{\omega^2 - \omega_l^2}{\omega^2 - \omega_t^2},$$

and substituting it in eq. (33) results in energy-loss rate:

$$-\frac{dW}{dt} = \int dk_\perp \frac{Q^2}{k_\perp} \omega_l^2 \left(\frac{\epsilon_0^{-1} + \epsilon_b^{-1}}{\epsilon_\infty^{-1} + \epsilon_b^{-1}}\right) \left(\frac{1}{\epsilon_\infty} - \frac{1}{\epsilon_0}\right) [\epsilon_b(\epsilon_\infty^{-1} + \epsilon_b^{-1})(\epsilon_0^{-1} + \epsilon_b^{-1})]^{-1}$$

$$\times \delta\left[\omega_t \left(\frac{\epsilon_0^{-1} + \epsilon_b^{-1}}{\epsilon_\infty^{-1} + \epsilon_b^{-1}}\right)^{1/2} - k_\perp \cdot v_\perp\right]. \tag{34}$$

Upon comparing the quantum and classical expressions for the energy loss rates, eqs. (24) and (34), we conclude that the optic longitudinal surface phonon frequency is given by

$$\Omega_l = \omega_l \left[\frac{\epsilon_0^{-1} + \epsilon_b^{-1}}{\epsilon_\infty^{-1} + \epsilon_b^{-1}}\right]^{1/2}, \tag{35}$$

where Ω_l is always smaller than ω_l. We also obtain that:

$$|N_{kl}|^2 = \frac{A}{(2\pi)^2} \frac{1}{2\pi k_\perp} \frac{\hbar\Omega_l(\epsilon_\infty^{-1} - \epsilon_0^{-1})}{\epsilon_b(\epsilon_\infty^{-1} + \epsilon_b^{-1})(\epsilon_0^{-1} + \epsilon_b^{-1})}. \tag{36}$$

Using our eq. (22) we obtain for the potential on the surface $z \approx 0$

$$\phi_s = A^{-1/2} \sum_k (-\mathrm{i}) \left[\frac{2\pi}{k_\perp} \frac{\hbar\Omega_l(\epsilon_\infty^{-1} - \epsilon_0^{-1})}{\epsilon_b(\epsilon_\infty^{-1} + \epsilon_b^{-1})(\epsilon_0^{-1} + \epsilon_b^{-1})}\right]^{1/2}$$
$$\times \exp(-k_\perp |z|) \exp(\mathrm{i}k_\perp \cdot r - \mathrm{i}\Omega_l t)\, a_{k_\perp} + \mathrm{h.c.} \tag{37}$$

For electrons which are bound to move on the surface of the crystal we have

$$\rho_e = e \sum_s \delta(z)\, \delta(r - r_s),$$

where r_s represent the electronic coordinates. The interaction Hamiltonian of this two-dimensional electron gas with surface phonons is given by

$$H_{\mathrm{int}} = \int \mathrm{d}r\, \rho_e\, \phi_s,$$

and reads:

$$H_{\mathrm{int}} = A^{-1/2} \sum_s \sum_{k_\perp} (-\mathrm{i}) \left[\frac{2\pi e^2}{k_\perp} \frac{\hbar\Omega_l(\epsilon_\infty^{-1} - \epsilon_0^{-1})}{\epsilon_b(\epsilon_\infty^{-1} + \epsilon_b^{-1})(\epsilon_0^{-1} + \epsilon_b^{-1})}\right]^{1/2}$$
$$\times \exp(\mathrm{i}k_\perp \cdot r_s - \mathrm{i}\Omega_l t)\, a_{k_\perp} + \mathrm{h.c.} \tag{38}$$

The interaction Hamiltonian as given by eq. (38) represents the interaction of a two-dimensional electron gas with optic longitudinal vibration on the polar crystal interface.

3. Conclusion and discussion

Using the dielectric formulation we were able to determine the interaction between electrons bound to move on a surface of a polar semiconductor, and lattice vibrations. This interaction is the result of electrons absorbing or emitting surface phonons (optic-longitudinal). The interaction potential in an electron-phonon collision is given by:

$$v_{k_\perp} = -\mathrm{i} \left[\frac{2\pi e^2}{k_\perp} \frac{\hbar\Omega_l(\epsilon_\infty^{-1} - \epsilon_0^{-1})}{\epsilon_b(\epsilon_\infty^{-1} + \epsilon_b^{-1})(\epsilon_0^{-1} + \epsilon_b^{-1})}\right]^{1/2}. \tag{39}$$

The surface phonon frequency was also obtained and is defined in eq. (35) in terms of the bulk longitudinal phonon frequency. The electron–lattice time-independent interaction Hamiltonian can be written as

$$H_{\rm int} = A^{-1/2}\sum_{k_\perp} v_{k_\perp}\rho_{k_\perp}a_{k_\perp} + \text{h.c.}, \tag{40}$$

where

$$\rho_{k_\perp} = \sum_s \exp(i\boldsymbol{k}_\perp \cdot \boldsymbol{r}_s)$$

is the Fourier transform of the electronic density operator which can be represented by

$$\sum_p c^\dagger_{p+k_\perp} c_p\,,$$

where c_p ($c^\dagger_p$) are the usual destruction (creation) operators for the electron gas. The interaction Hamiltonian, eq. (40), is the appropriate one to use when electron–phonon processes are considered, for electrons that are bound to move on an insulator–semiconductor (polar) interface.

References

[1] F. Stern, Solid State Sci. 4 (1974) 499.
[2] H. Ezawa, S. Kawaji and K. Nakamura, Surface Sci. 27 (1971) 218; J. Appl. Phys. 13 (1974) 126.
[3] H. Ezawa, S. Kawaji, T. Kuroda and K. Nakamura, Surface Sci. 24 (1971) 659.
[4] F. Stern and W.E. Howard, Phys. Rev. 163 (1967) 816.
[5] T. Ando, J. Phys. Soc. Japan 38 (1975) 989.
[6] T.K. Lee, C.S. Ting and J.J. Quinn, Phys. Rev. Letters 35 (1975) 1089.
[7] B. Vinter, Phys. Rev. Letters 35 (1975) 1044.
[8] N. Tzoar, P.M. Platzman and A. Simon, Phys. Rev. Letters 36 (1976) 1200.
[9] D.K. Ferry, Surface Sci. 57 (1976) 218; 75 (1978) 86.
[10] R.H. Ritchie, Phys. Rev. 106 (1957) 874.
[11] R.H. Ritchie and A.L. Marusak, Surface Sci. 4 (1966) 234.
[12] J.I. Gersten and N. Tzoar, Phys. Rev. B8 (1973) 5671.
[13] This well known result can be found, for example, in: C. Kittel, Quantum Theory of Solids (Wiley, 1963) ch. 7.

PHYSICAL REVIEW B VOLUME 20, NUMBER 4 15 AUGUST 1979

High-frequency conductivity of a two-dimensional electron gas interacting with optical phonons

Narkis Tzoar
Department of Physics, The City College of The City University of New York, New York, New York 10031
(Received 16 January 1979)

We calculate the high-frequency conductivity for a two-dimensional electron gas interacting with optical lattice vibrations. The collision frequency and the optical mass normalization are obtained. The frequency dependence of the (inverse) collision time is presented.

I. INTRODUCTION

When a device of metal-insulator-semiconductor structure is biased, a large accumulation of electrons or inversion layer is produced on the surface of the semiconductor. When the energy bands are bent, as in the case of strong inversion, a potential well appears on the insulator-semiconductor interface which localizes the motion of the electrons normally to the surface. On the other hand, the electrons are free to move in the plane of the surface. Under strong enough bias, the localization of the electrons in the direction normal to the surface, which is characterized by the spread of their wave function, is much smaller than their average distance within the plane. We are thus permitted to use a two-dimensional model for the electron gas in which the electrons are free to move only in the plane of the semiconductor surface.[1]

In treating the response of the electron gas in our system to a dc electric field (transport theory) or an ac electric field (optical properties), collision processes of electrons with ions, impurities, or acoustic phonons have been mainly considered.[2] These can explain results obtained in semiconductors such as Ge and Si. However when compound semiconductors are used, such as InSb, GaAr, etc., which are partially ionic, the interaction of the electrons with longitudinal-optic phonons becomes important and cannot be neglected.[3] A similar situation exists for bulk electrons in compound semiconductors. The effect is particularly notable at low temperature for optical absorption when the photon frequency ω exceeds the longitudinal-optic-phonon frequency Ω_l. Here a new channel of absorption, i.e., a final state with an excited phonon, is operative and influences strongly the optical-absorption coefficient. In Sec. II we present the theory for the high-frequency conductivity of a two-dimensional electron gas with polar optical phonons.

In treating the electron-phonon interaction one should note that the electrons moving on the surface of the semiconductor will interact most strongly with surface rather than bulk phonons.[4] Surface phonons produce a large electrostatic potential in the insulator-semiconductor interface. The potential decreases exponentially to zero away from the interface. The eigenfrequencies of the surface phonons and their interaction with the electrons depend on bulk properties as well as on the dielectric properties of the insulating barrier.

II. CALCULATIONS OF THE CONDUCTIVITY

Our electron-phonon system is described by the Hamiltonian

$$H = H_0 + H_1 \ , \tag{1}$$

where

$$H_0 = \sum_p \epsilon_p a_p^\dagger a_p + \sum_q \omega_q b_q^\dagger b_q \tag{2}$$

and

$$H_1 = \frac{1}{2A} \sum_{p,p',q} v_q a_{p'+q}^\dagger a_{p'-q}^\dagger a_{p'} a_p + \frac{1}{A^{1/2}} \sum_{p,q} (C_q a_{p+q}^\dagger a_p b_q + \text{H.c.}) \ . \tag{3}$$

Here ϵ_p is the kinetic energy of an electron having momentum $\vec{p}$, ω_q is the wave-number-dependent longitudinal-optic frequency and a_p, $a_p^\dagger$ (b_q, $b_q^\dagger$) are the destruction and creation operators, respectively, of the electrons (phonons). The coupling term $v_q = 2\pi e^2/q$ is the Fourier transform of the Coulomb interaction for planar electrons and

$$C_q = -i \frac{2\pi e^2}{q} \hbar\omega_l [\epsilon_b(\epsilon_\infty^{-1} + \epsilon_b^{-1})^{3/2}(\epsilon_0^{-1} + \epsilon_b^{-1})^{1/2}]^{-1/2}$$

represents the electron–longitudinal-optic-phonon in-

 ©1979 The American Physical Society

teraction.

To evaluate the conductivity we start from the Kubo formula which reads

$$\sigma(\omega)=\frac{1}{2A}\int_0^\infty d\tau\, e^{i\omega\tau}\int_0^\beta d\lambda\,\langle\vec{j}(\tau-i\lambda)\cdot\vec{j}(0)\rangle\ , \quad (4)$$

where ω is the frequency of the applied field, $\vec{j}(0)$ is the Fourier transform of the current operator for wave number equal to zero, and

$$\vec{j}(\tau)=e^{iH\tau}\vec{j}(0)e^{-iH\tau}\ . \quad (5)$$

The statistical average of an operator O is given by

$$\langle O\rangle=\mathrm{Tr}(e^{\beta(\Omega+\mu N-H)}O)\ , \quad (6)$$

where H is the total Hamiltonian of the system and Ω is defined by

$$e^{-\beta\Omega}=\mathrm{Tr}(e^{\beta(\mu N-H)})\ . \quad (7)$$

Here μ and N are the chemical potential and the number operator, respectively, and β is the inverse of the temperature in energy units.

In order to render Eq. (4) in a more convenient form, we integrate by parts and obtain

$$\sigma=\sigma_0+\sigma_1\ , \quad (8)$$

where

$$\sigma_0=i\frac{e^2n}{m\omega} \quad (9)$$

and

$$\sigma_1=\frac{1}{2\omega A}\int_0^\infty d\tau\, e^{i\omega\tau}\langle[\vec{j}(\tau),\vec{j}(0)]\rangle\ . \quad (10)$$

In Eq. (10) the square brackets denote the commutator.

Calculations of the current-current correlations and the conductivity in the three-dimensional case have been worked out in much detail and are well documented.[5] The calculations for the two-dimensional situation is remarkably similar and we shall present only the final results. We evaluate the conductivity treating electron-phonon collision within the Born approximation (high-frequency conductivity), however treating the self-consistent field of the fluctuating electron gas exactly in the random-phase approximation (RPA). Our expression includes the full dynamic screening of the electrons. We however will consider here a weak electron-phonon interaction and ignore completely the renormalization of the phonon spectrum and line broadening by the electron density fluctuations. Our result for the conductivity reads

$$\sigma=i\frac{ne^2}{m\omega}+\frac{e^2}{2\omega^3m^2(2\pi)^2}\int d\vec{q}\,q^2|C_q|^2\frac{P}{4\pi}\int_{-\infty}^{+\infty}dx\coth\left(\frac{\beta x}{2}\right)\frac{1}{\epsilon_q(x+\omega)}$$
$$\times\left\{\frac{1}{\epsilon_q(x)}[Q_q(x+\omega)-Q_q(x)][D_q(x+\omega)-D_q(x)]\right.$$
$$\left.-\frac{1}{\epsilon_q^*(x)}[Q_q(x+\omega)-Q_q^*(x)][D_q(x+\omega)-D_q^*(x)]\right\}\ . \quad (11)$$

Here the dielectric function is given by

$$\epsilon_q(x)=1-v_qQ_q(x)\ , \quad (12)$$

where Q, the density fluctuation is defined by

$$Q_q(x)=\frac{1}{(2\pi)^2}\int d\vec{p}\,\frac{f_{p+q/2}-f_{p-q/2}}{\epsilon_{p+q/2}-\epsilon_{p-q/2}-x-i\eta}\ . \quad (13)$$

$D_q(x)$ represents the phonon propagator and is given by

$$D_q(x)=\frac{2\omega_q}{x^2-\omega_q^2}\ . \quad (14)$$

To render our result for the conductivity in a more transparent form we shall identify the effect of the electron-phonon collision with the Drude form of the conductivity. We write for σ,

$$\sigma=i\frac{ne^2}{(m+\delta m)(\omega+i\nu)}\ , \quad (15)$$

where δm, the mass renormalization, and ν, the collision frequency, are small quantities. We therefore identify them as

$$\nu=(8\pi^2\omega mn)^{-1}\,\mathrm{Re}\int d\vec{q}\,q^2|C_q|^2\frac{1}{4\pi}$$
$$\times P\int_{-\infty}^{+\infty}dx\coth\left(\frac{\beta x}{2}\right)F\ , \quad (16)$$

$$\delta m=-(8\pi^2\omega^2n)^{-1}\,\mathrm{Im}\int d\vec{q}\,q^2|C_q|^2\frac{1}{4\pi}$$
$$\times P\int_{-\infty}^{+\infty}dx\coth\left(\frac{\beta x}{2}\right)F\ , \quad (17)$$

where

$$F=\frac{1}{\epsilon_q(x+\omega)}\left[\frac{1}{\epsilon_q(x)}[Q_q(x+\omega)-Q_q(x)][D_q(x+\omega)-D_q(x)]\right.$$
$$\left.-\frac{1}{\epsilon_q^*(x)}[Q_q(x+\omega)-Q_q^*(x)][D_q(x+\omega)-D_q^*(x)]\right] . \quad (18)$$

In order to calculate the collision frequency ν we shall use two simplified assumptions which are well justified. First we omit all phonon lifetime effects, thus ignoring the narrow spread of the phonon spectrum for any wave number q. Second, since the momentum transfer q is of the order of the Fermi momentum which in turn is much smaller than lattice momentum, we ignore entirely the dispersion of the phonons and replace ω_q by Ω_l, the longitudinal vibration frequency. After some algebra one obtains

$$\nu=(8\pi\omega mn)^{-1}\int dq\, q^3\left[\frac{|C_q|^2}{v_q}\right]$$
$$\times\left\{\left[\coth\left[\frac{\beta\Omega_l}{2}\right]+\coth\frac{\beta}{2}(\omega-\Omega_l)\right]\mathrm{Im}\frac{1}{\epsilon_q(\omega-\Omega_l)}+\left[\coth\left[\frac{\beta\Omega_l}{2}\right]+\coth\frac{\beta}{2}(\omega+\Omega_l)\right]\mathrm{Im}\frac{1}{\epsilon_q(\omega+\Omega_l)}\right\} . \quad (19)$$

For most practical situations, the temperature is smaller than the Fermi energy. We therefore are justified in taking the dielectric function at zero temperature. The statistical factor can also be taken at the zero-temperature limit for $k_BT<\hbar\Omega_l$. We thus obtain for the collision frequency at $T=0$,

$$\nu=(4\pi\omega mn)^{-1}\int dq\, q^3\left[\frac{|C_q|^2}{v_q}\right]\mathrm{Im}\left[\frac{1}{\epsilon_q(\omega-\Omega_l)}\right]\Theta(\omega-\Omega_l) . \quad (20)$$

Here, as expected, a threshold for absorption occurs at $\omega=\Omega_l$. The collision frequency rises for $\omega\gtrsim\Omega_l$ and, as we shall see later, behaves as $\omega^{-3/2}$ at high frequencies. The effect of finite temperature when $k_BT<\hbar\Omega_l$ would be mainly to round off the sharp threshold at $\omega=\Omega_l$. Numerical integration of Eq. (20) will be presented later.

The mass renormalization δm can be cast into a simpler form after some algebra and reads

$$\delta m=(8\pi^2\omega^2n)^{-1}\int dq\, q^3\left[\frac{|C_q|^2}{v_q}\right]\int_0^\infty dx\coth\left[\frac{\beta x}{2}\right]$$
$$\times\left[\mathrm{Im}\frac{1}{\epsilon_q^*(x)}\mathrm{Re}[D_q(x+\omega)+D_q(x-\omega)-2D_q(x)]\right.$$
$$\left.+\mathrm{Im}D_q(x)\,\mathrm{Re}\left[\frac{1}{\epsilon_q(x+\omega)}+\frac{1}{\epsilon_q(x-\omega)}-\frac{2}{\epsilon_q(x)}\right]\right] . \quad (21)$$

Numerical calculations of δm as a function of frequency are more difficult than for ν. Here the various terms in the integrand have alternating signs, thus large cancellations do occur. Let us determine the qualitative behavior of δm as a function ω. Here for $\omega\to\infty$, $\epsilon_q(x\pm\omega)$ may be replaced by unity and $D_q(x\pm\omega)$ asymptotically approaches zero as ω^{-2}. We thus conclude that for $\omega\to\infty$ the integral in Eq. (21) approaches a constant and hence $\delta m\sim\omega^{-2}$. On the other hand for $\omega\to0$ (below the longitudinal phonon frequency) the integrand in Eq. (21) behaves as ω^2, and thus δm becomes a constant when ω approaches zero. A detailed behavior of δm as a function of ω will not be presented here.

We go back now to our Eq. (20) and evaluate the collision frequency ν. Here we consider the situation where the Fermi energy is larger than k_BT and therefore are justified in using for $\epsilon_q(\omega-\Omega_l)$ the zero-temperature dielectric function. Our result reads

$$\frac{\nu}{\omega_l}=\frac{1}{2}(\lambda\tilde{c})\frac{1}{\Omega}\int_0^\infty dz\, z\frac{F(z,\Omega-\tilde{\Omega}_l)}{\epsilon(z,\Omega-\tilde{\Omega}_l)}\theta(\Omega-\tilde{\Omega}_l) , \quad (22)$$

where ω_l is the longitudinal-optic-phonon frequency, $\tilde{\Omega}_l$ is the surface phonon frequency, $\lambda=[2e^2m/\hbar^2(\pi n)^{1/2}]$ is the plasma parameter of the two-dimensional electron gas and

$$\tilde{c}=\frac{\epsilon_\infty^{-1}-\epsilon_0^{-1}}{\epsilon_b(\epsilon_\infty^{-1}+\epsilon_b^{-1})^{3/2}(\epsilon_0^{-1}+\epsilon_b^{-1})^{1/2}}$$

is the dielectric form factor for the interaction of the

electrons with surface phonons. Here $\Omega = \omega/4\epsilon_F$ and $z = q/2k_F$ are, respectively, the frequency and wave numbers normalized with respect to the Fermi energy and momentum. Also $\tilde{\Omega}_l$ is the surface phonon frequency similarly normalized. The integrand in Eq. (22) is given by

$$F(z,x) = D_-\left[1-\left(z-\frac{x}{z}\right)^2\right]^{1/2} - D_+\left[1-\left(z+\frac{x}{z}\right)^2\right]^{1/2},$$

$$D_\pm = \begin{cases} 0, & \text{if } |z \pm \frac{x}{z}| \geq 1, \\ 1, & \text{if } |z \pm \frac{x}{z}| < 1, \end{cases} \tag{23}$$

and

$$\epsilon(z,x) = 1 + \frac{\lambda}{z}\left[G(z,x) + i\frac{1}{2z}F(z,x)\right], \tag{24}$$

where

$$G(z,x) = \left\{1 - \frac{C_-}{2z}\left[\left|\left(z-\frac{x}{z}\right)^2 - 1\right|^{1/2} - \frac{C_+}{2z}\left[\left|\left(z+\frac{x}{z}\right)^2 - 1\right|^{1/2}\right]\right\},$$

$$C_\pm = \begin{cases} 0, & \text{if } |z \pm \frac{x}{z}| \leq 1, \\ \dfrac{z \pm (x/z)}{|z \pm (x/z)|}, & \text{if } |z \pm \frac{x}{z}| > 1. \end{cases}$$

Equation (22) can now be integrated using InSb parameters: $\omega_l = 24.4$ meV, $\epsilon_0 = 17.9$, $\epsilon_\infty = 15.7$, and as an example for the oxide layer, $\epsilon_b = 10$ is taken as a reasonable value. The Fermi energy in our calculation is taken to be 100 meV. In this case we obtain for the surface phonon

$$\Omega_l = \omega_l\left(\frac{\epsilon_0^{-1} + \epsilon_b^{-1}}{\epsilon_\infty^{-1} + \epsilon_b^{-1}}\right)^{1/2} = 0.95\omega_l,$$

which is almost equal to ω_l. Our result for ν as a function of the normalized frequency is presented in Fig. 1. The collision frequency ν is zero for frequencies below the surface phonon frequency. When the light frequency exceeds the surface phonon frequency, ν increases fast up to a constant value and remains so until $\omega = 4\omega_F$. Thereafter ν approaches asymptotically to a constant times $\omega^{-3/2}$, for large ω. This asymptotic form of ν is obtained when screening effects are omitted, i.e., when in Eq. (22) we replace $\epsilon(z, \Omega - \tilde{\Omega}_l)$ by unity.

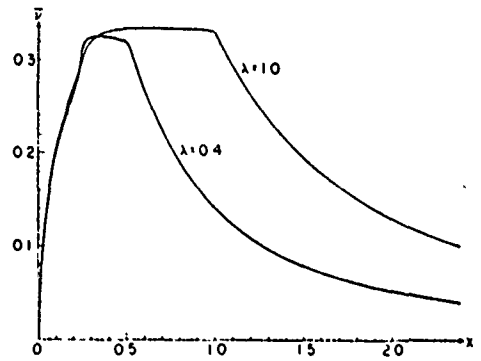

FIG. 1. Normalized collision frequency $\bar{\nu} = 2\nu/\lambda\tilde{C}\omega_l$ as a function of $\bar{x} = (\omega - \Omega_l)/4\omega_F$ for InSb at zero temperature, for $\lambda = 0.4$ and $\lambda = 1$.

In conclusion, we have calculated the collision frequency for a two-dimensional electron gas interacting with optical lattice vibrations. Our result for the collision frequency as a function of the photon energy is plotted in Fig. 1. We find that metal-oxide-semiconductor devices, made up of polar semiconductors, will exhibit a jump in the collision frequency when the photon frequency exceeds the optical-phonon frequency.

ACKNOWLEDGMENTS

This research was sponsored in part by the U.S. ONR under ONR Grant No. N00014-75-C-0949 and by The City University Faculty Award Program. We would like to thank A. L. Simon for the numerical calculations.

[1]F. Stern, Solid State Sci. 4, 499 (1974).

[2]H. Ezawa, S. Kawaji, and K. Nakamura, Surf. Sci. 27, 218 (1971), J. Appl. Phys. 13, 126 (1974), H. Ezawa, S. Kawaji, T. Kuroda, and K. Nakamura, Surf. Sci. 24, 659 (1971); F. Stern and W. E. Howard, Phys. Rev. 163, 816 (1967), T. Ando, J. Phys. Soc. Jpn. 38, 989 (1975), T. K. Lee, C. S. Ting, and J. J. Quinn, Phys. Rev. Lett. 35, 1048 (1975); B. Vinter, Phys. Rev. Lett. 35, 1044 (1975), N. Tzoar, P. M. Platzman, and A. Simon, Phys. Rev. Lett. 36, 1200 (1976).

[3]D. K. Ferry, Surf. Sci. 57, 218 (1976), 75, 86 (1978); A. Darr and J. P. Kotthaus, Magnetotransport in an Inversion Layer on p-InSb, Proceedings of the International Conference on "Electronic Properties of Two-Dimensional Systems", Berchtesgarden, Germany, Sept. 1977 (unpublished).

[4]Here we note that the surface longitudinal-optic-phonon frequency is given by $\Omega_l = \omega_l(\epsilon_0^{-1} + \epsilon_b^{-1})^{1/2}(\epsilon_\infty^{-1} + \epsilon_b^{-1})^{-1/2}$ where ω_l is the bulk phonon frequency and ϵ_b is the dielectric constant of the insulator or the oxide.

[5]N. Tzoar, Phys. Rev. 132, 202 (1963); 133, A1213 (1964); A. Ron and N. Tzoar, Phys. Rev. 133, A1378 (1964).

PHYSICAL REVIEW B VOLUME 20, NUMBER 10 15 NOVEMBER 1979

High-frequency conductivity of a two-dimensional, two-component electron gas

N. Tzoar
City College of the City University of New York, New York, New York 10031

P. M. Platzman
Bell Laboratories, Murray Hill, New Jersey 07974

(Received 30 January 1979)

A first-principles calculation of the high-frequency conductivity for a two-dimensional, two-component electron gas is presented. Both frequency and temperature dependence are considered. The influence of electron-electron collisions on the two-dimensional plasmon is discussed in relation to possible experiments in MOS structures.

I. INTRODUCTION

Recently, there has been considerable experimental and theoretical interest in the physics of electrons in so-called metal-oxide-semiconductor (MOS) structures.[1] In these devices, electrons are bound by the application of an applied electric field to the oxide-semiconductor interface. The potential they experience depends in detail on the field, the carrier concentration, and on the dielectric properties of the sandwich. It suffices to say that the effect of this potential is to quantize motion perpendicular to the structure into a set of discrete levels or subbands with spacing of the order of 100 °K. The motion in the plane of the interface is nearly free-electron-like with an effective mass characteristic of the three-dimensional (3-D) band structure. At low temperatures, this sytem behaves in many ways like an almost ideal 2-D electron gas. The fact that its density may be varied over many orders of magnitude by simply changing the applied electronic field has made it an interesting system for the study of Coulomb-interaction effects among electrons.

The high-frequency conductivity of such a system reflects many of its important physical properties. In fact, it has been known for some time that the cyclotron resonance line, or lines, in such systems depends in a rather complicated way on the carrier density, the frequency of the experiment, the temperature, and the orientation of the interface relative to the crystal axis.[2] Several attempts to understand the behavior of such cyclotron-resonance experiments within the framework of an interacting 2-D electron-gas picture have been made.[3] All such discussions except one[4] are based on a picture wherein a single group of carriers interacts with one another and with impurities. These calculations, roughly speaking, give an adequate description of the cyclotron resonance linewidth, the presence of subharmonics, and in some cases, the position of the line as a function of carrier concentration.

One set of experiments on Si(100) MOS structures have shown that the temperature dependence for $5\,^{\circ}\mathrm{K} < T < 80\,^{\circ}\mathrm{K}$ is anomalous. If we take this one experiment at face value, we are forced to conclude that the single resonance line moves from a position determined by an effective mass of $0.2m_e$ to an effective mass near $0.35m_e$ as the temperature is raised. Attempts to understand this effect within the conventional many-body picture discussed in the preceding paragraph have failed miserably. In fact, estimates of the temperature effect which rely on a single-species interacting Coulomb liquid suggest that the mass should become lighter as the temperature is raised.[3]

Fortunately, for Si(100), the situation is somewhat more complicated than our simple discussion would indicate. In this case, the multiellipsoidal nature of the 3-D band structure gives rise to two sets of subbands in the 2-D case. One of these, the lowest, had a 2-D mass of roughly $0.2m_e$ while the second set has a cyclotron mass of roughly $0.4m_e$. Appel and Overhauser[1] have recently used this fact to discuss the temperature dependence of the cyclotron resonance line. Using a set of *macroscopic* transport equations for the current along with an effective electron-electron relaxation time, they were able to show that one could qualitatively understand the CR experiments as a collisionally averaged line for the two groups of carriers. Of course, there is still some question of whether this is the correct interpretation of the data. The idea, however, is an interesting one and seems to deserve further *microscopic* analysis.

In this paper, we present a first-principles calculation of the high-frequency conductivity $\sigma(\omega)$ of a two-component degenerate system.[6] The

calculation is strictly valid to lowest order in $\lambda/2 \equiv r_s \equiv e^2 m/\hbar^2 k_F$, where m and k_F are the mass and Fermi wave vector of the light carrier. It properly includes all the dynamic screening effects. The results will be useful for interpreting the far-infrared Drude-type conductivity of the inversion layers. As we shall see, correlation effects which appear in the conductivity will influence the position and linewidth of the 2-D plasmon resonances which have been observed.[7]

II. FORMULATION

The Hamiltonian of our system is given by

$$H=\sum_{\vec{p},\alpha}\frac{p^2}{2m_\alpha}a^\dagger_{\vec{p},\alpha}a_{\vec{p},\alpha}+\tfrac{1}{2}\sum_{\vec{q},\vec{p}',\vec{p},\alpha}v_q a^\dagger_{\vec{p}+\vec{q},\alpha}a^\dagger_{\vec{p}'-\vec{q},\alpha'}a_{\vec{p}',\alpha'}a_{\vec{p},\alpha}. \tag{1}$$

In Eq. (1), $a_{\vec{p},\alpha}$ ($a^\dagger_{\vec{p},\alpha}$) is the destruction (creation) operator of electrons of type "α" having a momentum $\vec{p}$ and $v_q = 2\pi e^2/q$ is the Fourier transform of the Coulomb interaction between electrons confined to move in a plane.

Rigorous solution for the conductivity for the full range of frequencies is difficult to obtain. However, for the high-frequency conductivity, where $\omega\tau > 1$ (τ some effective collision time), a solution for $\sigma(\omega)$ was obtained in the 3-D case.[6] Here, collisions between particles having large momentum transfer are treated within the Born approximation. However, interaction effects within the Hartree approximation are considered to all orders. We thus treat the local field effect exactly, i.e., in the full random-phase approximation (RPA).

The calculation of the conductivity in the 2-D case can be carried out in a similar fashion to the 3-D case, which is well documented. The final result of such a calculation is

$$\sigma(\omega)=i\frac{e^2 n}{m\omega}\left(1+\frac{m}{M}\frac{N}{n}\right)\left[1+2\lambda^2\frac{(M/m)(1-m/M)^2}{1+(m/M)(N/n)}\frac{1}{\Omega^2}\int_0^\infty z\,dz\,\mathrm{P}\int_{-\infty}^{+\infty}dx\,F(x,z,\omega)\right]. \tag{2}$$

The correction to σ [second term in Eq. (2)] vanishes when $m = M$. This is a consequence of the general theorem that the long-wavelength conductivity is the noninteracting conductivity when the particles all have the same mass, i.e., conservation of momentum implies that the total current is conserved.[8]

In Eq. (2), $n, m, (N, M)$ are respectively the "light" electron ("heavy electron) density and mass, and $\Omega \equiv \omega/4E_F$ where E_F is the light-electron Fermi energy. Also, $z = q/2k_F$ represents the momentum transfer in the collision process. The retardation effects are represented by the integration over x (P is the principal value), which is the Fourier transform over the time in our normalized energy units.

The function F is quite complicated and has a statistical factor depending on $\beta = 4E_F/k_B T$ where k_B is the Boltzmann constant and T the temperature. The rest of the terms in our expression for F represent the long-wavelength current fluctuations in terms of the convolution of the density fluctuations of the light and heavy electrons. It reads

$$F=i\coth\frac{\beta x}{2}\,\epsilon_z^{-1}(x+\omega)\{\epsilon_z^{-1}(x)[G_z(x+\omega)-G_z(x)][J_z(x+\omega)-J_z(x)]-\epsilon_z^{*-1}(x)[G_z(x+\omega)-G_z^*(x)][J_z(x+\omega)-J_z^*(x)]\}. \tag{3}$$

Here $G_z(x)$ [$J_z(x)$] is proportional to the density fluctuations of the light (heavy) electrons and is given by

$$G_z(x)=G_z^R(x)+iG_z^I(x), \tag{4}$$

where

$$G_z^R(x)=1-\frac{C_-}{2z}[(z-x/z)^2-1]^{1/2}-\frac{C_+}{2z}[(z+x/z)^2-1]^{1/2},$$

$$C_\pm=\begin{cases}0, & \text{if } |z\pm x/z|\le 1\\ \dfrac{z\pm x/z}{|z\mp xz|}, & \text{if } |z\pm x/z|>1\end{cases} \tag{5}$$

and

$$G_z^I(x)=\frac{1}{2z}\left|D_-[1-(z-x/z)^2]^{1/2}-D_+[1-(z+x/z)^2]^{1/2}\right|,$$

$$D_\pm=\begin{cases}0, & \text{if } |z\pm x/z|\ge 1\\ 1, & \text{if } |z\pm x/z|<1.\end{cases} \tag{6}$$

Similarly,

$$J_z(x)=J_z^R(x)+iJ_z^I(x) \tag{7}$$

and

$$J_z^{R,I}(x)=G_z^{R,I}(x)\left[z-z\left(\frac{n}{N}\right);x-x\frac{M}{m}\left(\frac{n}{N}\right)\right]. \tag{8}$$

The dielectric function $\epsilon_z(x)$ is defined for our system as

$$\epsilon_z(x) = 1 + \frac{\lambda}{z}\left[G_z(x) + \frac{M}{m}J_z(x)\right]. \quad (9)$$

Our result for the high-frequency conductivity, Eq. (2), to lowest order in the plasma parameter is given in terms of F, Eq. (3), and represents the interaction between the density fluctuations of the light and heavy electrons including their dynamical screening. Although, at first sight, our result looks complicated, it represents a simple pysical process for absorption. Since G and J are proportional to the light and heavy electron density fluctuation, respectively [see Eq. (9)], the final state after absorption includes a light electron-hole pair as well as a heavy electron-hole pair The absorption process is as follows: The incoming photon excites, for example, the light electron-hole pair which, in turn, via the Coulomb interaction, excites a heavy electron-hole pair. Similarly, the photon may excite a heavy electron-hole pair which is followed by the excitation of a light electron-hole pair via the Coulomb interaction. Note that there is no final state with either two light electron-hole pairs or two heavy electron-hole pairs. These final states do not contribute to the absorptive part of the long-wavelength conductivity. Also note that in the limit of $m = M$ (where no distinction between light and heavy electron occurs) there is no contribution to the absorption due to correlation effects. Thus our first-principles theory accounts correctly for the appropriate final state and also takes into account the complicated dynamical screening represented here by the two factors of ϵ^{-1}, which makes Eq. (3) look complicated.

The exact evaluation of the double integral in Eq. (2) is quite complicated. We may use a simplified form for F which proved to be numerically acceptable in the three-dimensional case. We found that when the frequency ω was smaller than ω_p, some mean plasma frequency dynamical screening effects are not very important. In this case, it was possible to replace $\epsilon_z(x)$ by its static value. In this limit, Eq. (3) becomes

$$F = \frac{i\coth\beta\nu/2}{|\epsilon_z(0)|^2}\{[G_z(x+\omega) - G_z(x)][J_z(x+\omega) - J_z(x)] - [G_z(x+\omega) - G_z^*(x)][J_z(x+\omega) - J_z^*(x)]\}. \quad (10)$$

There is still an interesting physical question present in our choice of $\epsilon_z(0)$. Formally [see Eqs. (5) and (8)],

$$\epsilon_z(0) = 1 + \frac{\lambda}{z}(1 + M/m). \quad (11)$$

We have static screening from both carriers and that screening is independent of the number of those carriers. This is true because the *static* screening length in a 2-D degenerate system is independent of the number of carriers. We will be interested in the case where there is a variable number of heavy carriers. In particular, the appropriate response time (plasma frequency) for the small number of heavy carriers will be small compared to the applied frequency. In this case, it is a much better approximation to neglect the screening from the heavier carriers altogether, i.e., we pick $\epsilon_z(0) \simeq 1 + (\lambda/z)G_z^R(0)$.

After some algebra and use of the symmetry properties of $G^{R,I}$ and $J^{R,I}$ and the fact that we integrate over x, we find that the reactive or real part of F can be written as

$$F^R = \coth\left(\frac{\beta\nu}{2}\right)\{G_z^I(x)[J_z^R(x+\Omega) + J_z^R(x-\Omega) - 2J_z^R(x)] + (G \rightarrow J)\} \quad (12)$$

(in the second term, G and J are interchanged). The imaginary or absorptive term can be cast into the form

$$F^I = \left[\coth\frac{\beta\nu}{2} - \coth\frac{\beta}{2}(x-\Omega)\right]G_z^I(\Omega - x)J_z^I(x). \quad (13)$$

Using Eqs. (12) and (13), the conductivity Eq. (2) can be written as

$$\sigma = i\frac{e^2 n}{m}\left(1 + \frac{m}{M}\frac{N}{n}\right)\left(1 + \frac{(M/m)(1 - m/M)^2}{\left(1 + \frac{m}{M}\frac{N}{n}\right)\left(\frac{n}{N} + \frac{M}{m}\right)} \times \frac{\nu_R(\omega) + i\nu_I(\omega)}{i\Omega}\right), \quad (14)$$

where the complex frequency-dependent collision frequency

$$\nu_{R,I} = 2\left(\frac{n}{N} + \frac{M}{m}\right)\lambda^2\frac{1}{\Omega} \times \int_0^\infty z\,dz \int_0^\infty dx \frac{1}{|1 + (\lambda/z)G_z^R(0)|^2}F_{I,R}. \quad (15)$$

We have evaluated Eq. (15) numerically for a range of frequency and temperatures for $m/M = 1/2$, $n/N = 4$, and $\lambda = 1$. We find that the real part of the collision frequency (F_I) can be approximated by

$$\nu \simeq \nu_R(\Omega) = 2.4\left[\Omega^2 + 40\left(\frac{k_B T}{E_F}\right)^2\right]. \quad (16)$$

The functional form of the results is to be expected. The Ω^2 and T^2 dependence is simply related to the smallness of the phase space available to pairs of colliding particles having an energy transfer Ω. Our result for the collision frequency

was obtained using microscopic calculations for the response of the plasma to the radiation field. It incorporates, in principles, the dynamical correlation effects of the self-consistent field generated by the charged particles. However, for small frequencies and temperatures when only low-frequency density fluctuations are important, our numerical results are essentially similar to those presented by Appel and Overhauser. The numerical coefficients, of course, depend on all the details, such as the number of particles, mass ratios, etc. It seems inappropriate to study the dependence on these parameters without some experimental data with which to compare them.

The imaginary or reactive part of the collision frequency is quite different. It is not very temperature dependent. It has a magnitude at small Ω which is comparable to ν_R at $\Omega = 0.01$. Thus, for any physically interesting situation, it will be quantitatively unimportant. We will neglect it. Thus, our first-principles calculation of the conductivity shows us that for frequencies high compared to the collision frequency itself, but low compared to the Fermi energy, one must use a frequency-dependent real ν [see Eq. (14)]. At lower frequencies (low compared to ν itself), a macroscopic semiphenomenological treatment of σ (see Appendix) similar to that used in Ref. 1 leads to a simple form for σ, for all frequencies, i.e.,

$$\sigma = i\frac{e^2 n}{m\omega}\left(1+\frac{m}{M}\frac{N}{n}\right)\left(1+\frac{(M/m)(1-m/M)^2}{\left(1+\frac{m}{M}\frac{N}{n}\right)\left(\frac{n}{N}+\frac{M}{m}\right)}\frac{\nu}{i\Omega-\nu}\right). \tag{17}$$

For low enough frequencies, the conductivity develops a reactive part as a result of correlations. This reactive part will lead to a shift of the observed 2-D plasma frequency. For values of the parameters used in the numerical evaluation and assuming $\hbar\omega < k_B T < E_F$,

$$\sigma \cong i\sigma_0\left\{1+\frac{1}{27}\left[\frac{22.5(k_B T/E_F)^2}{i\omega-22.5(k_B T/E_F)}\right]\right\}. \tag{18}$$

There will be about a 4% shift in the plasmon frequency for $\omega < (22.5)(k_B T)^2/E_F$ and a Lorentzian-type contribution to the linewidth as a function of T or ω of the same order of magnitude. Both such effects should be observable.

ACKNOWLEDGMENTS

We would like to thank S. J. Allen and D. Tsui for a number of interesting discussions on possible experimental consequences of our calculations, and A. L. Simons for the numerical calculations. The research of one of us (N.T.) was sponsored by the U. S. Office of Naval Research under ONR Grant No. N00014-75-C-0949.

APPENDIX: CALCULATIONS OF CONDUCTIVITY FOR CONSTANT COLLISION TIME

We consider here an interacting system of light and heavy electrons. As is well known, a long wavelength radiation field cannot be absorbed due to the collision between electrons having the same mass. Thus, no relaxation process involving either of the species is possible. The collision between the light and heavy electrons is effective as long as their relative momentum is not zero. For equal numbers of electrons, the relative momentum is given by $(Mp - mP)/(m+M)$ where lower case and capital letters refer to the different densities n and N of the two types of electrons. The kinetic equation reads

$$\dot{\vec{p}} = -enE - \frac{nNmM}{nm+NM}\left(\frac{\vec{p}}{nm}-\frac{\vec{P}}{NM}\right)\frac{1}{\tau}. \tag{A1}$$

The second term on the right-hand side of Eq. (A1) represents the relaxation of relative momentum for a constant electron collision time. Similarly, we obtain

$$\dot{\vec{P}} = -eNE - \frac{nNmM}{nm+NM}\left(\frac{\vec{P}}{NM}-\frac{\vec{p}}{nm}\right)\frac{1}{\tau}. \tag{A2}$$

The solution for the velocities $v = p/m$ and $V = P/M$ for a field of the form $E e^{i\omega t}$ involves some algebra but is not difficult to obtain. Given the velocities, we can evaluate the current density $j = e(v+V)$ and use $\sigma = j/E$ to obtain our final result. The conductivity $(1/\tau = \nu)$ is

$$\sigma = i\frac{e^2 n}{m\omega}\left(1+\frac{m}{M}\frac{N}{n}\right) \times\left(1+\frac{(M/m)(1-m/M)^2}{\left(1+\frac{m}{M}\frac{N}{n}\right)\left(\frac{n}{N}+\frac{M}{m}\right)}\frac{\nu}{i\Omega-\nu}\right). \tag{A3}$$

In other words, Eq. (17) appropriately extends our high-frequency result to the collision-dominated regime, i.e., it is consistent with kinetic theory when a constant collision time is considered.

[1]Proceedings of the Second International Conference on Electronic Properties of 2-D Systems, Berchtesgaden, 1977 published in Surf. Sci. 73 (1978).
[2]T. A. Kennedy, R. J. Wagner, R. D. McCombe, and D. Tsui, Phys. Rev. Lett. 35, 1031 (1975).
[3]N. Tzoar, P. M. Platzman, and A. Simons, Phys. Rev. Lett. 36, 1200 (1976); C. S. Ting, S. C. Ying, and T. J. Quinn, *ibid.* 37, 215 (1976); T. Ando, *ibid.* 36, 1383 (1976).
[4]J. Appel and A. W. Overhauser, Phys. Rev. B 18, 758 (1978).
[5]H. Kubleck and J. P. Kotthaus, Phys. Rev. Lett. 35, 1019 (1975).
[6]N. Tzoar and P. M. Platzman, in *Linear and Non-Linear Electron Transport in Solids*, edited by J. T. Devreese and V. E. Van Doren (Wiley, New York, 1976).
[7]Marc Baus, Phys. Rev. Lett. 40, 793 (1978).
[8]W. Kohn, Phys. Rev. 123, 1242 (1961).